2012

# Novel biological, forensic, and historical applications of inductively coupled plasma-mass spectrometry

Megan Louise Mekoli
*Iowa State University*

# Novel biological, forensic, and historical applications of inductively coupled plasma-mass spectrometry

by

Megan Louise Mekoli

A dissertation submitted to the graduate faculty

in partial fulfillment of the requirements for the degree of

DOCTOR OF PHILOSOPHY

Major: Analytical Chemistry

Program of Study Committee:
R. Sam Houk, Major Professor
Ning Fang
Young-Jin Lee
Patricia Thiel
L. Keith Woo

Iowa State University

Ames, Iowa

2012

## Table of Contents

## Abstract

This dissertation describes three new applications of inductively coupled plasma mass spectrometry (ICP-MS).

Arsenic content was measured in rice and coffee samples. These results for the concentration of arsenic in rice and coffee independently verify the results of a similar FDA study. Direct comparisons of the arsenic content in different types of rice (i.e. black, brown, jasmine) indicated no correlation in the amount of arsenic and the type of rice. Additionally, the rice and coffee samples were cultivated in different locations throughout the world and results were analyzed to discern any trends between the amount of arsenic and the country of origin.

Laser ablation inductively coupled plasma mass spectrometry (LA-ICP-MS) is used to measure the trace elemental composition of various well-known brands of duct and electrical tapes. A new method derived from existing chemometric principles (principal components analysis) for identifying which elements vary the most between the brands of tape is described. The new method is applied to measurements collected from duct and electrical tapes and they are compared to one another.

Pigments from a ship which sank off the coast of Texas in 1684 were recently recovered. ICP-MS was used to perform elemental analysis on these samples to identify the type of pigment. These pigments were suspected to be products for trade with natives in the new world. As was common at the time, the pigments were also suspected of adulteration (being cut with a cheaper product); they were analyzed for evidence of such a practice.

ICP-MS is one of the most sensitive useful tools for elemental analysis. Knowing the exact composition of various samples using this technique can help scientists assist in setting

new public safety standards in the present, provide new techniques for the future, and learn about life in the past. The three applications highlight the versatility of ICP-MS to a broadening number of different scientific disciplines.

# Chapter 1. Introduction

## ICP-MS

### *Intro and General Advantages*

Inductively coupled plasma mass spectrometry (ICP-MS) is one of the most powerful, sensitive, and versatile techniques for elemental analysis. It is used for a number of different applications in various scientific disciplines including forensics, [1] geology, [2] archaeology, [3, 4] environmental chemistry, [5] semiconductors, [6] and nanomaterials. [7] One of the main advantages of this instrument over other chemical analysis techniques is its ability to achieve accurate and precise ultra-trace measurements of multiple elements in a variety of samples. Detection limits for ICP-MS are commonly in the low part-per-billion (ng/g) to parts-per-trillion (pg/g) range depending on the background signal and the element of interest. ICP-MS also has the distinct advantage of exhibiting a large dynamic range. Additionally, the ability of ICP-MS to detect element signals from Li to U in the periodic table makes this a versatile technique for elemental analysis.

### *Inductively Coupled Plasma*

Figure 1 is a schematic of an inductively coupled plasma torch. The ICP is an atmospheric ionization source which vaporizes, atomizes and ionizes samples at high temperatures (5000-8000 K). [8, 9] Argon is generally the gas used to create the plasma as it has a high ionization potential energy (15.76 eV), [10] is inert, and does not readily form complex molecular ions with sample matter in the plasma. The plasma is created and shaped by the ICP torch. Fused quartz was chosen as the material for the torch because it has a low

coefficient of thermal expansion ($5.5\times10^{-7}$/°C) and a high melting point (~1700 °C), [11] which allows it to withstand large, rapid changes in temperature without cracking.

The torch contains three concentric channels. Argon that flows through the outer channel (outer gas, ~1 L/min) and the middle channel (auxiliary gas, ~16 L/min) is used to stabilize, shape, and regulate the temperature of the plasma. The outer and auxiliary gas flows may be independently controlled to achieve the desired plasma. The central channel is where the sample gas carries the sample aerosol into the plasma.

To create the plasma, a radio frequency (RF) wave (27 or 40 MHz) is applied to a coil with 2 to 4 turns located around the outside of the torch at the downstream end. The plasma power is typically operated at 1200 W, but may be changed depending on the desired plasma conditions. Cool plasmas used for the reduction of polyatomic species generally operate with a much lower forward power.

A spark provides initial free electrons, which collide with and ionize the Ar gas. This process creates more free electrons. The resultant free electrons collide with other Ar atoms and sample molecules effectively atomizing and ionizing them.

The most common form of sample introduction into the plasma is by solution nebulization. Solutions are typically nebulized into a spray chamber and the resultant aerosol is sent into the centermost tube of a quartz torch, where it is vaporized, atomized and ionized in the plasma.

***Mass Spectrometer***

Sample ions and gas are extracted from the plasma through a series of cones: the sampler and the skimmer, which are commonly made of Pt, Ni, or Al. These cones shape the

ions into a narrow beam and provide an interface for the differential pumping system. Using ion optics, the ion beam is accelerated and shaped to allow passage through the entrance slit to the mass analyzer.

There are several different types of mass analyzers that may be used for ion separation in conjunction with ICP. From the mass analyzer, the ions travel into the detector where the ion signal is converted into an electronic signal, which is amplified and finally detected.

The mass analyzer used in all three areas of this work is called a magnetic sector, which can be seen in Figure 2. The particular model seen in Figure 2 is an ELEMENT 1 (Thermo, inc.) magnetic sector. This particular model has a reverse Nier-Johnson geometry where ions are first separated according to their various momenta by the magnet and then are focused to pass through the exit slit and onto the detector based on their respective kinetic energies by an electrostatic analyzer (ESA). A magnetic sector with a Nier-Johnson geometry has the components switched, where ions are first separated according to their kinetic energies by an ESA followed by additional separation by the magnet based on each ion's momentum. Magnetic sector instruments have a range of available operating mass resolutions ($m/\Delta m$ = 300, 4000, or 10000) that are achieved by varying the entrance and exit slit widths. The width of the high resolution slit is only 10 μm wide; barely visible to the naked eye. However, there is a trade-off of decreasing ion throughput and therefore decreasing signal with increasing resolution.

A multi-channel (MC) mass analyzer combines the high mass resolution ion separation technique of magnetic sector geometry with several separate detectors called Faraday cups. This type of mass analyzer is unique in that simultaneous measurements of

signals from different masses may take place, thus, increasing the sensitivity of analyte ions, obtaining better accuracy of isotope ratios, and negating the need for fast electronic switching.

***Polyatomic Interferences***

ICP-MS typically produces singly-charged monatomic ions, however this is not always the case. Incomplete atomization and ionization of matter in the plasma or inelastic collisions can lead to detection of polyatomic ions in the MS. These polyatomic ions can have approximately the same m/z value as singly charged monotomic analyte ions, worsening precision and accuracy of the analysis. Common polyatomic ions typically consist of some form of metal argide ($MAr^+$), metal oxide ($MO^+$), or metal hydride ($MH^+$) ionic species because argon, oxygen, and hydrogen are the most abundant elements found in the plasma besides sample matter. [12] The occurrence of these ions in the plasma depends on several different factors such as the bond dissociation energy of the species, the abundance of the neutral elements entering the plasma and the temperature of the plasma.

There are a variety of ways to reduce these polyatomic ions to increase precision and accuracy of analyte signal. One solution is to increase the plasma temperature enough to eliminate these interferences; however, this will also increase the prevalence of doubly charged atomic ions, which in turn, can interfere with analyte signal. [13]

One particular example of a polyatomic interference is that of $^{40}Ar^{16}O^+$ (m/z 55.95729), which interferes with the most abundant isotope of iron, $^{56}Fe^+$ (m/z 55.93494). The resolution required to separate these two ions from one another is only 2500, which can be achieved using a commercial instrument. Increasing the resolution can distinguish analyte

signal from polyatomic interference signals. However, the analyte signal must be high as there is a trade-off of decreasing sensitivity with increasing resolution. There are instances where even the best commercial instrument is not able to resolve two signals. Like the case of $^{102}Ru^{+}$ (m/z 101.90435) and $^{86}Sr^{16}O^{+}$ (m/z 101.90418) which requires a resolution of approximately 600,000 to separate the signals.

$MO^{+}$ and $MH^{+}$ species typically originate from the use of water as a solvent. A desolvation system like an Apex (Elemental Scientific Inc., Omaha, NE) can increase analyte sensitivity by drastically decreasing the number of water molecules injected into the plasma. [14, 15]

**MEMORY EFFECTS**

Samples with high amounts of volatile elements such as Hg, Cd, I, Pb and Li suffer from undesirable memory effects, which cause long washout times and decreased sensitivity over time. [16 17 18] Mercury is a volatile element that will adhere to the walls of the spray chamber and sample tubing and can volatilize later, decreasing accuracy. Thorium is a non-volatile element that is not expected to suffer similar effects as Hg, but does in practice for unknown reasons. [19] However, it has been determined that Th will only adhere to- and volatilize from the walls of the spray chamber and not the sample tubing. [20] There have been many attempts to reduce memory effects from volatile elements such as the use of a desolvation system (i.e. apex), [15] a flow injection sample introduction system, [21] an isotope dilution cold vapor technique, [22] microsampling, [23] and pre-treatment with a reducing agent. [24]

## SAMPLE PREPARATION

Liquid samples for analysis by ICP-MS typically are aqueous in nature as organic solvents can destabilize and extinguish the plasma. [25] Samples are commonly acidified and diluted using aqueous acids to keep elements in solution and achieve a stable signal from the instrument.

### *Dissolution*

Solid samples can be dissolved using strong aqueous acids such as nitric acid ($HNO_3$), hydrochloric acid (HCl), sulfuric acid ($H_2SO_4$), or hydrofluoric acid (HF). Considerations for choosing the best acid for dissolution depend on the sample matrix and what will keep the element of interest in solution.

If the acid does not keep the analyte in solution, problems with detection can occur. Large particles could clog the nebulizer and sample would not be introduced into the plasma. Another problem associated with poorly dissolved samples is agglomerations of analyte that may enter the plasma, atomize and ionize all at once, causing spikes and poor signal stability. Conversely, analyte agglomerations from poorly dissolved sample may not all be completely atomized and ionized and thus will not be detected, causing misrepresentation of the true analyte content in the sample.

Sometimes microwave digestion is necessary to heat the sample and acid under intense pressure in a closed vessel. Microwave digestion is effective at dissolving samples because heating increases the solubility of metals and the speed of sample decomposition while lowering the pressure in the relatively much cooler, Teflon vessel. [26]

### *Clean Techniques*

As ICP-MS is very sensitive, clean techniques such as sub-boiling acid distillation and acid vapor washing of Teflon containers must be employed to reduce contamination from acid, solvent (i.e. water), and sample containers. [27, 28] Sub-boiling distillation is a technique used to clean acids by gently heating one end of an L-shaped tube containing one type of contaminated acid. The clean acid vapor will condense on the cool, unheated bend and collect in the other end of the tube, which is located in a bucket of cool water. Gentle heating is required for this technique because low boiling-point elements (such as Hg) can be easily vaporized and end up in the "clean" acid.

Solutions must be stored in clean Teflon containers instead of glass because glass tends to leach metals and contaminate samples, especially in the presence of acids. [28] Additionally, Teflon sample containers must be cleaned by a process called acid vapor washing. [27] Basically, acid vapor washing is a form of gently refluxing concentrated nitric acid from a plastic bottle into an upturned Teflon bottle being cleaned on top.

## LASER ABLATION

Another form of sample introduction is ablation of solid samples using a laser. In the laser ablation used here, a beam of 266 nm laser light is focused onto the surface of a sample in a closed ablation cell and the resulting sample matter is swept through a tube to the ICP by a carrier gas. Laser ablation can be more advantageous than solution-based introduction systems because little to no sample preparation is required. [29] Additionally, spatial information may be collected for sample imaging. [30, 31, 32]

One caveat of laser ablation is in order for an accurate analysis, samples must be homogeneous, have a flat surface for effective ablation, and must be compared to matrix-matched standards. [33]

***Carrier Gas***

Typically Ar is used as the carrier gas for laser ablation, however studies have shown the advantages of using He, rather than Ar. Helium has a larger thermal conductivity than Ar, allowing it to disperse heat away from the ablation site thereby reducing fractionation (defined here as the discrepancy of the actual sample stoichiometry from the detected stoichiometry). [34, 35] He has also been shown to reduce the redeposition of ablated sample material back onto the sample. [36]

***Pulse Length***

Traditionally, lasers with a pulse length in the nanosecond (ns) range have been used for laser ablation, however lasers with femtosecond (fs) pulse length are more effective, with better precision and accuracy than ns lasers. [37] The short length of time of a single pulse for a fs laser is not long enough to allow the sample to dissipate the energy into the sample as heat. [38] The longer pulse-length of ns lasers imparts more energy that dissipates as heat into the sample. Due to this heat dissipation, ablation using ns lasers can lead to sample melting and undesirable fractionation effects. [39] Particulate matter ejected from the surface of a sample during fs laser ablation is much smaller in size, and more uniform than that of ns ablation. [40] Recently, there has been a photographic study comparing matter being ionized and atomized

in the ICP from a ns laser and a fs laser which shows that aerosol from the fs laser is easily ionized, with fewer large particles than that of ns lasers. [41]

## DISSERTATION ORGANIZATION

This dissertation is organized into five chapters. The first chapter provides a general introduction to ICP-MS and laser ablation. Chapter 2 is a manuscript detailing the determination of As in dissolved rice grains and coffee bean samples that were cultivated in different countries throughout the world. This chapter independently confirms the arsenic content in rice to that of the FDA findings. In chapter 2, the country of sample origin was not correlated with arsenic content. Similarly, there was no correlation between the arsenic content in any particular type of rice analyzed (i.e. black, brown, jasmine, etc.)

Chapter 3 is a manuscript prepared for submission into *The Journal of Forensic Science*. It describes a new application of utilizing principal component analysis (PCA, a multivariate statistical technique) to identify trace elements which contribute the most variance to distinguishing between different samples. Additionally, this new method was utilized on data taken from laser ablation ICP-MS measurements to perform a head-to-head comparative trace-elemental analysis of the backing and adhesive sides for four different brands of duct and electrical tapes.

Chapter 4 is a manuscript for a chapter called "Pigments" to be published in a book titled: *La Belle: The Archaeology of a 17$^{th}$ Century Ship of New World Colonization.* It describes an elemental analysis and chemical identification of suspected vermilion pigments taken from a French ship which sank off the coast of Texas around 1684. Chapter 5 is a summary of conclusions from the above studies.

**FIGURES**

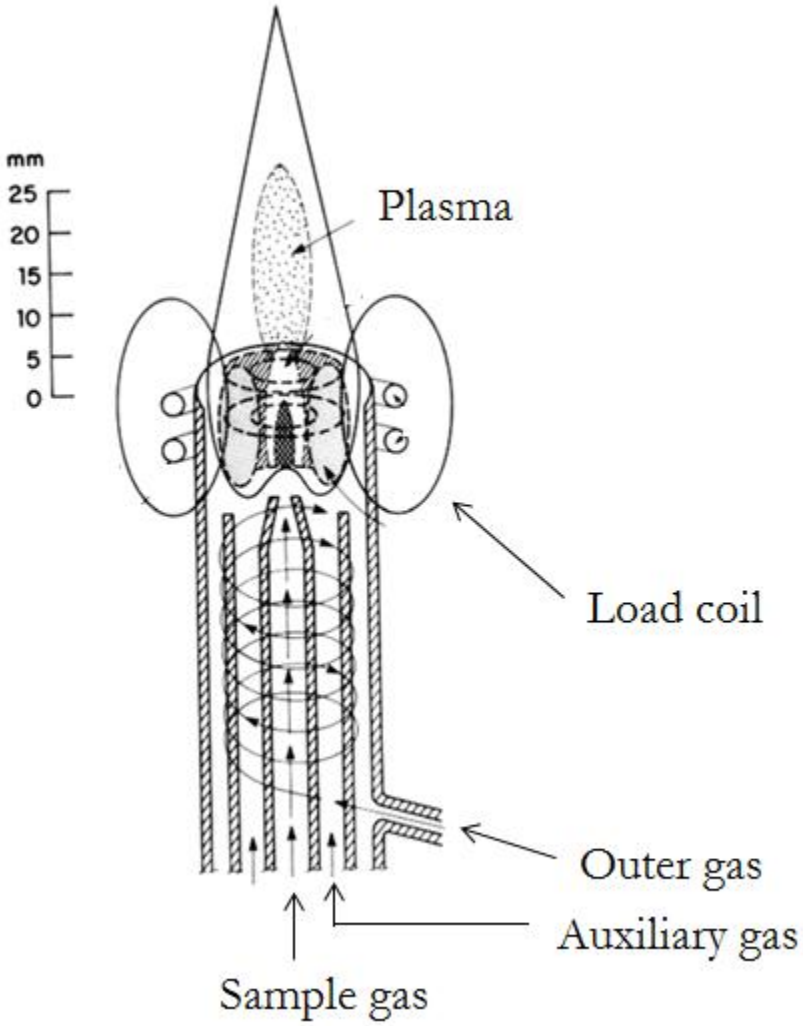


**Figure 1** Schematic of the inductively coupled torch. The plasma created in this fused quartz torch vaporizes, atomizes, and ionizes samples that are sent through the middle channel by the sample gas. [42]

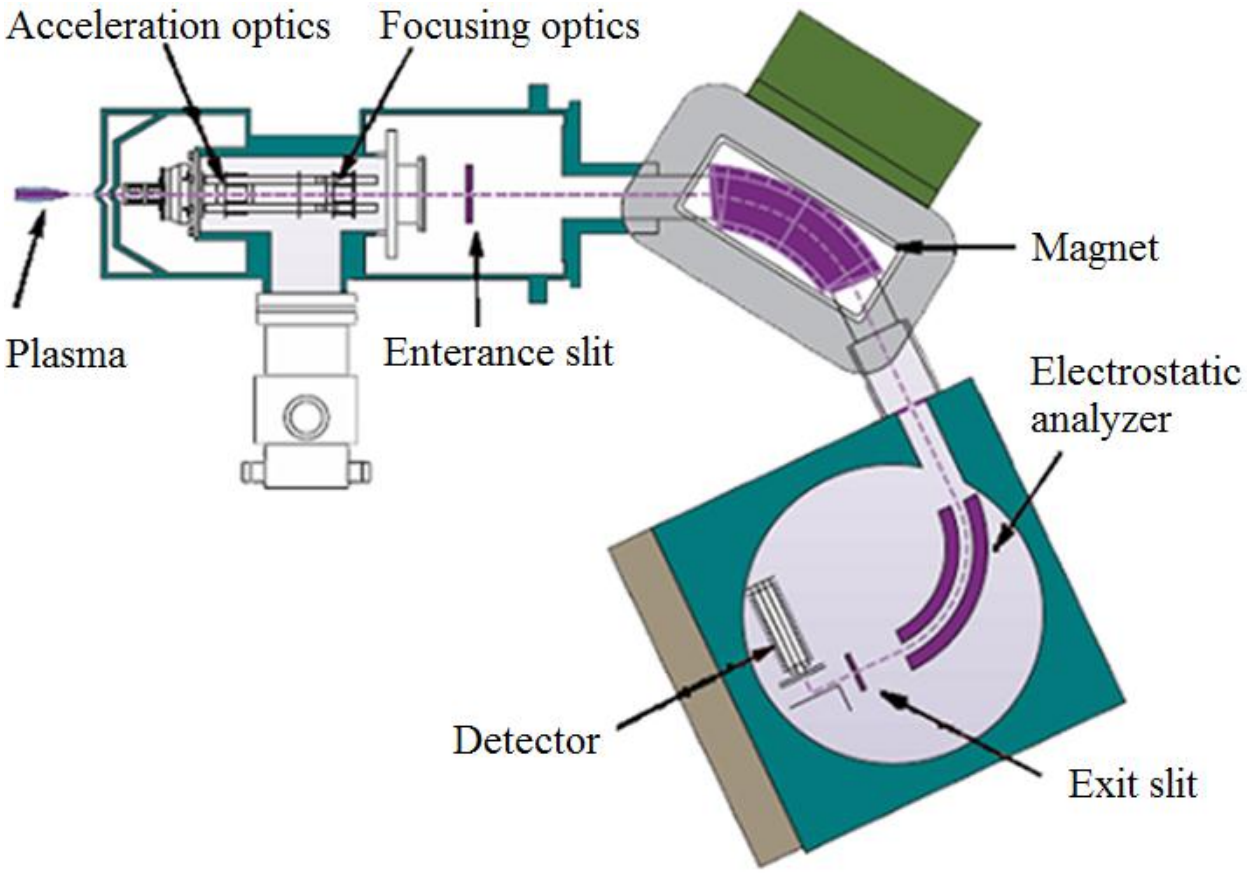


**Figure 2** Double focusing ICP-MS device. Ions are separated first by their respective momenta and then refocused by the electrostatic analyzer based on their respective kinetic energies. [43]

## REFERENCES

1. Bajic, S. J.; Aeschliman, D. B.; Saetveit, N. J.; Baldwin, D. P.; Houk, R. S. Analysis of Glass Fragments by Laser Ablation-Inductively Coupled Plasma-Mass Spectrometry and Principal Component Analysis. *J. Forensic Sci.* **2005,** *50,* 1123-1127.

2. Linge, K. L. Recent Developments in Trace Element Analysis by ICP-AES and ICP-MS with Particular Reference to Geological and Environmental Samples. *Geostand. and Geoanal. Research* **2005,** *29,* 7-22.

3. Resano, M.; Garcia-Ruiz, E.; Vanhaecke, F. Laser Ablation-Inductively Coupled Plasma Mass Spectrometry for the Investigation of Archaeological Samples. In *Mass Spectrometry Handbook;* Lee, M. S., Ed.; John Wiley & Sons: Hoboken, 2012; pp 829-843.

4. Olofsson, A.; Rodushkin, I. Provenancing Flint Artefacts with ICP-MS Using Ree Signatures and Pb Isotopes as Discriminants: Preliminary Results of a Case Study from Northern Sweden. *Archaeometry* **2011,** *53,* 1142-1170.

5. Skorek, R.; Jablonska, M.; Polowniak, M.; Kita, A.; Janoska, P.; Buhl, F. Application of ICP-MS and Various Computational Methods for Drinking Water Quality Assessment from the Silesian District (Southern Poland). *Cent. Eur. J. of Chem.* **2012,** *10,* 71-84.

6. Shabanti, M. B.; Shiina, Y.; Kirscht, F. G.; Simanuki, Y. Recent Advanced Applications of AAS and ICP-MS in the Semiconductor Industry. *Mat. Sci. & Eng. B: Solid-State Mat. for Adv. Tech.* **2003,** *B102,* 238-246.

7. Tsutsumi, Y.; Yoshioka, Y. Quantifying the Biodistribution of Nanoparticles. *Nat. Nanotech.* **2011,** *6,* 755.

8. Houk, R. S.; Thompson, J. J. Inductively Coupled Plasma Mass Spectrometry. *Mass Spec. Rev.* **1988,** *7,* 425-461.

9. Jarvis, K. E.; Gray, A. L. *Handbook of Inductively Coupled Plasma Mass Spectrometry;* Chapman and Hall: New York, 1992.

10. Niu, H.; Houk, R. S. Fundamental Aspects of Ion Extraction in Inductively Coupled Plasma Mass Spectrometry. *Spectrochim. Acta Part B* **1996,** *51,* 779-815.

11. Oishi, J.; Kimura, T. Thermal Expansion of Fused Quartz. *Metrologia* **1968,** *5,* 50-55.

12. Houk, R. S.; Parphairaksit, N. Dissociation of Polyatomis Ions in the Inductively Coupled Plasma. *Spectrochim. Acta Part B* **2001,** *56,* 1069-1096.

13. Jarvis, K. E.; Gray, A. L.; McCurdy, E. Avoidance of Spectral Interference on Europium in Inductively Coupled Plasma Mass Spectrometry by Sensitive Measurement of the Doubly Charged Ion. *J. Anal. Atom. Spec.* **1989,** *4,* 743-747.

14. Minnich, M. G.; Houk, R. S. Comparison of Cryogenic and Membrane Desolvation for Attenuation of Oxide, Hydride and Hydroxide Ions and Ions Containing Chlorine in

Inductively Coupled Plasma Mass Spectrometry. *J. Anal. Atom. Spec.* **1998,** *13*, 167-174.

15. Elemental Scientific Inc. *High Sensitivity Inlet System for ICP-OES & ICPMS;* Omaha.

16. Sun, X. F.; Ting, B. T.; Zeisel, S.; Janghorbani, M. Accurate Measurement of Stable Isotopes of Lithium by Inductively Coupled Plasma Mass Spectrometry. *Analyst* **1987,** *112*, 1223-1228.

17. Date, A. R.; Gray, A. L. *Applications of ICP-MS;* Chapman and Hall: New York, 1989.

18. Gelinas, Y.; Krushevska, A.; Barnes, R. M. Determination of Total Iodine in Nutritional and Biological Samples by ICP-MS Following Their Combustion with an Oxygen Stream. *Anal. Chem.* **1998,** *70*, 1021-1025.

19. Twiss, P.; Watling, R. J.; Delev, D. Determination of Thorium and Uranium in Fecal Material from Occupationally-Exposed Workers Using ICP-MS. *Atomic Spectrosc.* **1994,** *15*, 36-39.

20. Al-Ammar, A.; Reitznerova, E.; Barnes, R. M. Thorium and Iodine Memory Effects in Inductively Coupled Plasma-Mass Spectrometry. *Fresenius J. Anal. Chem* **2001,** *370*, 479-482.

21. Harrington, C. F.; Merson, S. A.; D'Silva, T. M. Method to Reduce the Effect of Mercury in the Analysis of Fish Tissue Using Inductively Coupled Plasma Mass Spectrometry. *Anal. Chim. Acta* **2004,** *505*, 247-254.

22. Christopher, S. J.; Long, S. E.; Rearick, M. S.; Fassett, J. D. Development of Isotope Dilution Cold Vapor Inductively Coupled Plasma Mass Spectrometry and Its Application to the Certification of Mercury in NIST Standard Reference Materials. *Anal. Chem.* **2001,** *73*, 2190-2199.

23. Fujimori, E.; Wei, R.; Sawatari, H.; Chiba, K.; Haraguchi, H. Multielement Determination of Trace Elements in Sediment Sample by Inductively Coupled Plasma Mass Spectrometry with Microsampling Technique. *Bulletin of the Chemical Society of Japan* **1996,** *69*, 3505-3511.

24. Meng, W.; Weiyue, F.; Junwen, S.; Fang, Z.; Bing, W.; Motao, Z.; Bai, L.; Yuliang, Z.; Zhifang, C. Development of a Mild Mercaptoethanol Extraction Method for Determination of Mercury Species in Biological Samples by HPLC-ICP-MS. *Talanta* **2007,** *71*, 2034-2039.

25. Pedersen, G. A.; Larsen, E. H. Speciation of Four Selenium Compounds Using High-Performance Liquid Chromatography with On-Line Detection by Inductively Coupled Plasma-Mass Spectrometry. *Fresenius' J. Anal. Chem.* **1997,** *358,* 591-598.

26. Kingston, H. M.; Jamie, L. B. *Introduction to Microwave Sample Preparation: Theory and Practice;* ACS Professional Reference Book: Washington, D.C., 1988.

27. Yuan, H.; Hu, S.; Tong, J.; Zhao, L.; Lin, S.; Gao, S. Preparation of Ultra-Pure Water and Acids and Investigation of Background of an ICP-MS Laboratory. *Talanta* **2000,** *52,* 971-981.

28. U.S. National Bureau of Standards. *Accuracy in Trace Analysis: Sampling, Sample Handling, and Analysis;* U.S. National Bureau of Standards: Washington, D.C., 1976.

29. Hattendorf, B.; Latkoczy, C.; Guenther, D. Laser Ablation-ICPMS. *Anal. Chem.* **2003,** *75,* 341A-347A.

30. Becker, J. S.; Zoiry, M.; Matusch, A.; Wu, B.; Salber, D.; Palm, C.; Becker, J. S. Bioimaging of Metals by Laser Ablation Inductively Coupled Plasma Mass SPectrometry (LA-ICP-MS). *Mass Spec. Rev.* **2009,** *29,* 156-175.

31. Becker, J. S.; Zoriy, M. W. B.; Matusch, A.; Becker, J. S. Imaging of Essential and Toxic Elements in Biological Tissues by LA-ICP-MS. *J. Anal. At. Spec.* **2008,** *23,* 1275-1280.

32. Kindness, A.; Sekaran, C. N.; Feldmann, J. Two-dimensional Mapping of Copper and Zinc in Liver Sections by Laser Ablation Inductively Coupled Plasma Mass Spectrometry. *Clinical Chem.* **2003,** *49,* 1916-1923.

33. Bian, Q.; Garcia, C. C.; Koch, J.; Niemax, K. Non-matrix Matched Calibration of Major and Minor Concentrations of Zn and Cu in Brass, Aluminum and Silicate Glass Using NIR Femtosecond Laser Ablation Inductively Coupled Plasma Mass Spectrometry. *J. Anal. Atom. Spectrom.* **2009,** *21,* 187-191.

34. Murphy, A. B. Transport Coefficients of Helium and Argon-Helium Plasmas. *IEEE T. Plasma Sci.* **1997,** *25,* 809-814.

35. Wang, Z.; Hattendorf, B.; Gunther, D. Analyte Response in Laser Ablation Inductively Coupled Plasma Mass Spectrometry. *J. Am. Soc. Mass Spectrom.* **2006,** *17,* 641-651.

36. Eggins, S. M.; Kinsley, L. P. J.; Shelley, J. M. G. Deposition and Element Fractionation Process During Atmospheric Pressure Laser Sampling for Analysis by ICP-MS. *Appl.*

*Surf. Sci.* **1998,** *129,* 278.

37. Fernandez, B.; Pecheyran, C.; Donard, O. F. X.; Claverie, F. Direct Analysis of Solid Samples by fs-LA-ICP-MS. *TrAC-Trend. Anal. Chem.* **2007,** *26,* 951-966.

38. Gonzalez, J.; Dundas, S. H.; Liu, C.; Mao, X.; Russo, R. E. UV-femtosecond and Nanosecond Laser Ablation-ICP-MS: Internal and External Repeatability. *J. Anal. Atom. Spetrom* **2006,** *21,* 778-784.

39. Hergenroder, R.; Samek, O.; Hommes, V. Femtosecond Pulse Shaping Using a Liquid-Crystal Display: Application to Deptch Profiling Analysis. *Mass Spectrom. Rev.* **2005,** *2005,* 086104.

40. Liu, C. Y.; Mao, X. L.; Mao, S. S.; Zeng, X.; Greif, R.; Russo, R. Nanosecond and Femtosecond Laser Ablation of Brass: Particulate and ICPMS Measurements. *Anal. Chem.* **2004,** *76,* 379-383.

41. Ebert, C. H.; Saetveit, N. J.; Zamzow, D. S.; Baldwin, D. P.; Bajic, S. J.; Houk, R. S. Digital Photographic Studies of Vaporization and Atomization in the Inductively Coupled Plasma with Fast Shutter Speed and High Framing Rate. Part II: Effects of Solid Particles from Laser Ablation at 266 nm with 10 ns and 150 fs Pulses Using Helium and Argon Carrier Gas. *J. Anal. Atom. Spec. In prep.*

42. Houk, R. S. Short Course on Inductively Coupled Plasma-Mass Spectrometry., 2012.

43. Thermo Finnigan Inc. Some Basic Aspects of High Resolution ICP-MS. (accessed 2012).

# Chapter 2: Determination of Total Arsenic in International Samples of Rice and Coffee by Inductively Coupled Plasma Mass Spectrometry

*Megan L. Mekoli and R. Sam Houk*

Ames Laboratory-U.S. Department of Energy, Iowa State University (ISU), Ames, Iowa, 50011-3020

## ABSTRACT

The concentration of As in coffee and rice samples was determined using solution-based inductively coupled plasma-mass spectrometry. Rice concentrations determined here were found to agree with those found in previous studies by the FDA [1] and Consumer Reports magazine [2]. Whole, uncooked rice grains were found to contain more As than coffee beans. One sample of rice in particular contained a very high concentration of total As. There was no correlation between total As content in rice and the country of origin. Additionally, there was no correlation between total As content in rice and the type of rice analyzed. In contrast, coffee beans cultivated in Uganda contained more As than coffee beans cultivated in other countries.

## INTRODUCTION

Recent published reports have indicated the total As content in rice grains and other rice-based food products can be alarmingly high. Rice (*Oryza sativa*) is a grass that is cultivated annually in warm climates. The processed (de-hulled) grains are a dietary staple

for much of the world's population. Rice is also used as a substitute for gluten containing grains in many processed foods for gluten-intolerant people.

With so much consumption of rice around the world, the content of toxic elements in rice is cause for concern. Recently, Consumer Reports [2] reported total As concentrations in rice in the range of hundreds of ppb. The FDA [1] also reported total As values in approximately 200 rice and rice product samples that were of similar concentration ranges to those reported by Consumer Reports.

There are two general classes of As compounds: inorganic and organic. Inorganic As is considered to be more dangerous than organic As because inorganic arsenic can cause a range of life-threatening diseases. [3] However, more recent studies indicate that organic As can also be harmful.

There are two oxidation states, for As in inorganic compounds: arsenite ($As^{III}$) and arsenate ($As^{V}$). Arsenic in arsenous acid, has a +3 oxidation state and has the chemical formula $As^{III}(OH)_3$.

Arsenous acid: $As(OH)_3 \Leftrightarrow H^+ + As(OH)_2O^-$ $pK_a = 9.22$ [1] [4]

The Arsenate ($As^{V}$) ion, $AsO_4^{3-}$, which has a +5 oxidation state, also has acid-base properties. Arsenic acid ($H_3AsO_4$) is a triprotic acid which has similar characteristics to phosphoric acid ($H_3PO_4$).

$H_3AsO_4 \Leftrightarrow H^+ + H_2AsO_4^-$ $pK_{a1} = 2.19$ [2]

$H_2AsO_4^- \Leftrightarrow H^+ + HAsO_4^{2-}$ $pK_{a2} = 6.94$ [3]

$HAsO_4^{2-} \Leftrightarrow H^+ + AsO_4^{3-}$ $pK_{a3} = 11.5$ [4] [4]

These highly toxic inorganic $As^{III}$ and $As^{V}$ compounds can be converted by bacteria into less toxic forms of organic As. Monomethylarsinic acid ($CH_5AsO_3$) dimethylarsinic

acid, ($(CH_3)_2AsO_2H$) and arsenobetaine, ($CH_3As^+CH_2COO^-$) are three of the most common organic compounds in nature that are widely considered to be less harmful as compounds containing $As^v$.

Inorganic arsenic is especially dangerous to life forms because it is chemically similar to phosphorus, which occurs in the same group of the periodic table. Phosphorus is an essential element to life and is in the sugar-phosphate backbone of DNA, it also participates in energy production as adenosine triphosphate (ATP). Arsenic disrupts these essential biomolecules by causing epigenetic changes to DNA such as excessive methylation, histone modification and interference with RNA. [5] Chronic human exposure to As has been shown to correlate with a range of life-threatening illnesses such as mild toxicity, cardiovascular disease, neurological defects, and cancer. [6]

The most common form of exposure to compounds containing As is ingestion of contaminated food and water. [7] There are currently limits on As concentrations in drinking water. The highest acceptable limit of total As in drinking water for the European Union is 10 ppb, [8] while 10 ppb is the highest acceptable limit for inorganic As in the US [9] and for the World Health Organization (WHO) [10]. Arsenic is a component in pesticides, herbicides, wood preservatives, coal burning, runoff from mineral mining, and waste from glass manufacturing that can end up in water and soil.

Over time, As can accumulate in soil and be taken up by crops meant for consumption by humans. It is possible that rice grown in paddies can be exposed to and take up even higher amounts of As from the free-standing water in which the plants are grown. [11, 12, 13] However, the US FDA does not currently have limits in place for total As in rice, but there has been recent legislation proposes such limits. [14]

Another possible source of As exposure is coffee. Coffee beans are classified as berries which grow on the outer region of the coffee plant, unlike rice, which grows within a husk. Whole coffee beans are typically not eaten, only steeped with hot water to extract flavor components. With the high water solubility of inorganic As, it could be particularly dangerous, as the process of making coffee could extract and concentrate this harmful toxin.

Total As in rice has typically been quantified by inductively coupled plasma-quadrupole mass spectrometry (ICP-qMS) with a collision cell. [15, 16] Total As can also be measured using magnetic sector ICP-MS [20] as is also the case here. Total As here was measured in low resolution using a magnetic sector ICP-MS. At low and medium resolutions ($m/\Delta m$=300 and 4000, respectively), there is a polyatomic ion signal at m/z 75 ($^{40}Ar^{35}Cl^{+}$), which interferes with the only As isotope at the same m/z value. Corrections are required to account for this interference when As signal is measured in low and medium resolutions on a magnetic sector ICP-MS. The use of high resolution ($m/\Delta m$=10000) on a magnetic sector ICP-MS instrument may distinguish these peaks. However, the small slit width used for high resolution lowers ion transmission that leads to signal loss of over 80% from that of low resolution; the signal using high resolution may be too low for detection.

Other ways of quantifying total As in rice have been by nanoscale secondary ion mass spectrometry (SIMS), [17, 16] synchrotron-X-ray fluorescence (S-XRF), [15] or in a few, very recent cases, by laser ablation (LA)-ICP-MS. [18, 19]

The study here determines if there are regional trends (i.e. distinct country-wide trends) of total As in rice and coffee or whether total As concentrations in these foods are more localized. Different types of rice such as black, brown or white rice, may possess different amounts of As. The type of rice analyzed is examined to discern any trends. A

magnetic sector ICP-MS is used to measure total As concentration in 12 samples of rice and 7 samples of coffee.

## METHODS

### *Samples*

Table 1 is a list of the rice and coffee samples along with information on their origins. Twelve samples of rice were purchased at local grocery stores and international markets in Ames. Samples were collected in categories of white, black, and brown rice from diverse international origins to discern possible trends in rice type and country of origin. Two samples, Lundberg long grain and Lundberg jasmine were marketed as "certified organic" from the Lundberg Family Farms in Richland, CA. [21] Seven brands of whole, dry-roasted coffee beans were purchased at a local co-op. These coffee beans were marketed as "fair trade" coffee with the country of origin clearly displayed.

### *Sample Preparation*

Coffee samples were individually ground using a clean, dry granite mortar and pestle for easier dissolution. Approximately 0.5 g of each sample was weighed into clean Teflon microwave digestion vessels along with approximately 10 g of clean sub-boiling distilled, 70% nitric acid. Rhenium was added to the concentrated nitric acid at 10 ppm as an internal standard (Alfa Aesar Specpure, Ward Hill, MA) to correct for incomplete transfer from the digestion process. The samples were digested using a microwave digestion system (MDS 2100, CDM, Matthews, NC). Table 2 is a list of operational parameters for the microwave digest system.

Approximately 600 µL of digested material was diluted to a final mass of approximately 30 g using ultrapure (17.4 MΩ, Millipore) water. Tungsten (1 ppm, High Purity Standards, Charleston, SC) was added during this step as an internal standard to monitor ICP-MS signal response and correct for matrix effects. The final concentration of digested material was approximately 1000 ppm and the concentrations of both the Re and W internal standards were approximately 10 ppb. A blank without rice or coffee from clean, microwave digested 70% nitric acid was also made in the same manner. Transfer recovery of Re from the digestion was 70% to 108% for the digestion of rice and 61% to 78% for coffee.

***ICP-MS***

Arsenic content of the dissolved and diluted samples was measured in low resolution ($m/\Delta m=300$) on a magnetic sector ICP-MS device (ELEMENT 1, Thermo, inc.). Instrumental operating parameters of the ELEMENT 1 ICP-MS device can be found in Table 3.

***Data Analysis***

Arsenic has one stable isotope at m/z 75, however, a polyatomic interference corresponding to $^{40}Ar^{35}Cl^{+}$ overlaps with the $^{75}As^{+}$ signal ($S_{As}$) at m/z 75. The samples of interest contain substantial levels of chlorine, so the $^{40}Ar^{35}Cl^{+}$ content must be adjusted using $^{40}Ar^{37}Cl^{+}$. Because $^{77}Se^{+}$ interferes with the $^{40}Ar^{37}Cl^{+}$ peak at m/z 77, the total signal of m/z 77 must also be adjusted using $^{82}Se^{+}$ at m/z 82. Krypton also has an interference at m/z 82, that is typically accounted for as it can often be present in Ar used for plasma generation, however in the experiment here, there was no observable Kr signal.

Signal intensity values at masses m/z 75, 77, 82 and 83 collected in low resolution from the ICP-MS were peak area integrated, averaged over 100 subsequent measurements and background subtracted.

The overall simplified expression for finding the adjusted arsenic signal ($S_{As}$) is:

$$S_{As}=S_{75} - 3.13S_{77} + 2.6S_{82} +0.84S_{83} \quad [5]$$

where $S_{As}$ is the actual signal of the arsenic, $S_{75}$ is the measured signal at m/z 75, $S_{77}$ is the measured signal at m/z 77, $S_{82}$ is the measured signal at m/z 82 and $S_{83}$ is the measured signal at m/z 83. In this case, $S_{83} = 0$. To determine concentration, the adjusted As signals ($S_{As}$) were compared to a 10 ppb standard solution of As (SCP Science, Champlain, NY), Re and W in 2% nitric acid.

## RESULTS AND DISCUSSION

Table 4 lists the concentration of As and the 1 sigma precision values in rice and coffee samples. The limit of quantitation (LOQ), defined here as ten times the measured integrated, averaged blank level, was found to be 0.23-2.07 ppb.

### *Rice*

The concentrations of total As in rice determined here are similar to what was found by others. [1, 2] The total As content of Carnaroli rice was found to be 122 ± 8 ppb. In a study recently published by the US FDA, [1] Carnaroli was a brand of rice that was analyzed for As content. In the FDA study, Carnaroli was found to contain 112 ppb of total As, not far below the average value determined here (122 ± 8 ppb). Uncertainty was not provided in the FDA

study, so exact agreement between of the reported concentration by the US FDA [1] and the concentration found here could not be determined.

Rice samples were collected with the specific goal of comparing As content from different international growing locations. In the samples analyzed here, there was not a clear trend between As concentration and the country of origin. Rice samples originating from Thailand contained varying concentrations of As, from 111 ± 6 ppb to 234 ± 15 ppb. Higher levels of As in water and soil have been reported in many areas of Thailand due to runoff from tin mining. [13] The varying levels of total As in rice from Thailand indicate that generalized country-wide statements could not be made regarding total As composition and it is likely that total As concentrations may be dependent on more localized conditions; however, in order to make definitive conclusions, As concentration in rice must be assessed relative to soil.

Also of interest is the basmati rice sample labeled Mekong Flower from Cambodia. This sample contained 412 ± 26 ppb, by far, the highest concentration of total As overall. According to Kohnhorst, [13] the Mekong River Delta soil, (a likely origin of this particular rice sample as it is named "Mekong Flower rice"), has a very high natural As abundance. More analyzed samples of rice originating from Cambodia would be necessary to confirm whether the rice originating from the Mekong delta has consistently higher As concentration than rice cultivated in other countries.

Samples from Lundberg Family Farms in CA, USA that were marketed as "certified organic rice" did contain lower concentrations of total As than many other international rice samples analyzed here that were not labeled as "certified organic rice". In the US, there are strict guidelines for certified organic farming, especially concerning the use of pesticides,

herbicides, and wood-preservation chemicals. Such regulations have been shown to add increased amounts of As. However, even in the certified organic rice samples, there are still detectible levels of As.

Multiple different types of rice were collected and analyzed to determine whether there are trends in total As content associated with a particular type of rice (i.e. black, brown, basmati, jasmine). Table 4 indicates the type of rice analyzed for each sample. There are no clear trends indicating any type of rice has consistently high or low amounts of As. From the samples analyzed here, it seems likely that As content in rice is not correlated with the type of rice cultivated.

***Coffee***

Coffee samples analyzed here generally contained far less total As than rice. There were two samples, C 4 from Peru and C 6 from Ethiopia, which did not contain measurable total As above the limit of detection (defined here as the sample concentration that yields a net signal 3 times the signal of the background: ~0.5 ppb in the dissolved sample).

There were two coffee samples analyzed which originated from Uganda. These samples contained the highest concentrations of total As measured here, 70 and 142 ppb. The total As concentration of the latter coffee sample was higher than that of half the rice samples analyzed.

The beans analyzed here were also of the caffeinated variety. The process of decaffeinating coffee beans involves steaming the whole beans and then extracting caffeine using organic solvents. Another interesting study could be conducted to determine if the decaffeination process changes total As content.

## CONCLUSION

The concentrations of total As in rice samples were found to be consistent with those published by the FDA and Consumer Reports.

The data reported indicate that total As content in rice can be dependent upon more localized soil compositions than a generalized country-wide region. With high restrictions put on food products marketed as “certified organic”, the analyzed certified organic rice samples generally contained lower concentrations of total As than many other samples analyzed here. However, these samples still contained measurable concentrations of total As, well over the limit of quantitation for this particular analysis.

There was no correlation between the concentration of As measured and the type of rice grain.

With the exception of sample C 5, coffee contained far lower concentrations of total As than rice samples. C 5, originating from Uganda contained an alarmingly high concentration of total As.

## TABLES

**Table 1** List of rice and coffee samples that were analyzed for As content.

| Rice Sample | Country of Origin | Type |
|---|---|---|
| Milagrosa | Thailand | Jasmine rice |
| Assi Rice | China | Black rice |
| Lundberg Long Grain | CA, USA | Brown rice |
| Lundberg Jasmine | CA, USA | Jasmine rice |
| Mekong Flower | Cambodia | Basmati rice |
| Forbidden | China | Black rice |
| Jade Pearl | CA, USA | White, polished rice |
| Carnaroli | Italy | Basmati rice |
| Volcano | Indonesia | White/brown mixed |
| Alter Eco | Thailand | Jasmine rice |
| Asian Taste | Thailand | Jasmine rice |
| Duru | Turkey | Basmati rice |

| Coffee Sample | Country of Origin | Type |
|---|---|---|
| C 1 | Ethiopia | Coffee |
| C 2 | Bolivia | Coffee |
| C 3 | Guatemala | Coffee |
| C 4 | Peru | Coffee |
| C 5 | Uganda | Coffee |
| C 6 | Ethiopia | Coffee |
| C 7 | Uganda | Coffee |

**Table 2** Parameters for microwave digestion of rice and ground coffee samples in Teflon

| Max Temperature | | 190 ˚C | | |
|---|---|---|---|---|
| **Microwave digestion program:** | | | | |
| Stage | Max pressure (PSI) | power (W) | Ramp time (min) | Time at set point (min) |
| 1 | 40 | 500 | 10 | 5 |
| 2 | 80 | 550 | 10 | 5 |
| 3 | 120 | 600 | 10 | 5 |
| 4 | 175 | 650 | 20 | 10 |

**Table 3** Instrumental parameters for ICP-MS device

| | |
|---|---|
| ICP-MS Instrument | ELEMENT 1 (Thermo, inc.) |
| Sampler and skimmer cones | Ni, H configuration (Thermo, inc.) |
| Sample gas | 1.06 L Ar $min^{-1}$ |
| RF Power | 1150 W |
| Outer/auxiliary gas stream | 16.00/1.16 L Ar $min^{-1}$ |
| Torch position, ion optics | Optimized for maximum sensitivity and stability |
| Scan mode<br>dwell/settling time | Peak jump, 10 points per mass, 10 ms dwell time,<br>2.1 ms settling time |
| Detection mode<br>Runs/passes | Counting<br>100 runs/1 pass |
| m/z values measured (low resolution, m/Δm=400) | 75, 77, 82, 182, 184, 185, 187 |

**Table 4** Concentration of total As in original rice samples

| Rice Sample | Total As conc. (ppb) | Precision (ppb) Std dev., n=100 | Country of Origin | Type |
|---|---|---|---|---|
| Lundberg jasmine | 69.5 | 4.4 | CA, USA | Jasmine rice |
| Volcano | 70.7 | 4.6 | Indonesia | Brown/White mixed rice |
| Milagrosa | 111 | 6.0 | Thailand | Jasmine rice |
| Lundberg long grain | 111 | 7.1 | CA, USA | Brown rice |
| Jade pearl | 119 | 7.5 | CA, USA | White, polished rice |
| Carnaroli | 122 | 7.8 | Italy | Basmati rice |
| Duru | 202 | 11 | Turkey | Basmati rice |
| Forbidden | 202 | 11 | China | Black rice |
| Alter Eco | 220 | 14 | Thailand | Jasmine rice |
| Assi | 228 | 13 | China | Black rice |
| Asian Taste | 234 | 15 | Thailand | Jasmine rice |
| Mekong flower | 412 | 26 | Cambodia | Basmati rice |

**Table 5** Concentration of total As in coffee

| Coffee Sample | Total As conc. (ppb) | Precision (ppb) Std. dev., n=100 | Country of Origin | Type |
|---|---|---|---|---|
| C 4 | < 0.5* | NA | Peru | Coffee |
| C 6 | < 0.5* | NA | Ethiopia | Coffee |
| C 3 | 12.49 | 0.87 | Guatemala | Coffee |
| C 2 | 32.80 | 2.12 | Bolivia | Coffee |
| C 1 | 63.51 | 4.76 | Ethiopia | Coffee |
| C 7 | 70.00 | 3.93 | Uganda | Coffee |
| C 5 | 141.94 | 7.62 | Uganda | Coffee |

*L.O.D. ≈ 0.5 ppb

**REFERENCES**


1. United States Food and Drug Administration. Arsenic in Rice: Full Analytical Results from Rice/Rice Product Sampling - September 2012. http://www.fda.gov/Food/FoodSafety/FoodContaminantsAdulteration/Metals/ucm319916.htm (accessed Oct 19, 2012).

2. Consumer Reports. Arsenic in Your Food. *Consumer Reports* **2012,** 22-27.

3. Abedin, M. D. J.; Cresser, M. S.; Meharg, A. A.; Feldmann, J.; Cotter-Howells, J. Arsenic Accumulation and Metabolism in Rice. *Environ. Sci. and Tech.* **2002,** *36,* 962-968.

4. Harris, D. C. *Quantitative Chemical Analysis,* 6th ed.; W.H. Freeman and Company: New York, 2003.

5. Baccarelli, A.; Bollati, V. Epigenetics and Environmental Chemicals. *Current Opinion In Pediatrics* **2009,** *21* (2), 243-251.

6. States, J. C.; Barchowsky, A.; Cartwright, I. L.; Reichard, J. F.; Futscher, B. W.; Lantz, R. C. Arsenic Toxicology: Translating Between Experimental Models and Human Pathology. *Environ. Health Persp.* **2011,** *119,* 1356-1363.

7. Reilly, C. In *Metal Contamination of Food;* Elsevier Science Publishers Ltd., 1991; p 284.

8. Council Directive 98/83/EC. *Offic. J. Europ. Commun,* May 15, 1998.

9. US EPA. Arsenic Drinking Water Standards. http://www.epa.gov/ (accessed October 22, 2012).

10. WHO. Guidelines for Drinking Water Quality, 3rd ed. http://www.who.int/water_sanitation_health/dwq/gdwq3rev/en/. (accessed October 22, 2012).

11. Onken, B. M.; Hossner, L. R. *J. Environ. Qual.* **1995,** *24,* 373-381.

12. Sapunar-Postruznik, J.; Bazulic, D.; Kubala, H. *Sci. Total Environ.* **1996,** *191,* 11-123.

13. Kohnhorst, A. Arsenic in Groundwater in Selected Countries in Sou and Southeast Asia: A Review. *J. Trop. Med. Parasitol.* **2005,** *28,* 73-82.

14. Hsu, T. Legislators Propose Limits on Arsenic in Rice. *Los Angeles Times,* September 2 2012.

15. Meharg, A. A.; Lombi, E.; Williams, P. N.; Scheckel, K. G.; Feldmann, J.; Raab, A.; Zhu, Y.; Islam, R. Speciation and Localization of Arsenic in White and Brown Rice Grains. *Environ. Sci. Technol.* **2008,** *42,* 1051-1057.

16. Moore, K. L.; Schroder, M.; Lombi, E.; Zhao, F. J.; McGrath, S. P.; Hawkesford, M. J.; Shewry, P. R.; Grovenor, C. R. M. *New Phytol.* **2010,** *185,* 434-445.

17. Carey, A.; Lombi, E.; Donner, E.; de Jonge, M. D.; Punshon, T.; Jackson, B. P.; Guerinot, M. L.; Price, A. H.; Meharg, A. A. A Review of Recent Developments in Speciation and Location of Arsenic and Selenium in Rice Grain. *Anal. Bioanal. Chem.* **2012,** *402,* 3275-3286.

18. Carey, A.; Norton, G. J.; Deacon, C.; Scheckel, K. G.; Lombi, E.; Punchon, T.; Guerinot, M. L.; Lanzirotti, A.; Newville, M.; Choi, Y.; Price, A. H.; Meharg, A. A. *New Phytol.* **2011,** *192,* 87-98.

19. Basnet, P.; Amarasiriwardena, D. Bioimaging of Trace Metal Distribution in Rice Seeds (Oryza Sativa) by LA-ICP-MS. *sciX*, Kansas City, MO, 2012.

20. D'Ilio, S.; Alessandrelli, M.; Cresti, R.; Forte, G.; Caroli, S. Arsenic Content of Various Types of Rice as Determined by Plasma-Based Techniques. *Microchem. J.* **2002,** *73,* 195-201.

21. Lundberg Family Farms. Lundberg Family Farms. http://www.lundberg.com/.

22. Taylor, R. G.; Howard, K. W. F. Groundwater Quality in Rural Uganda: Hydrochemical Considerations for the Development of Aquifers within the Basment Complex of Africa. In *Guondwater Quality;* Nash, H. a. M. G. J. H., Ed.; G.J.H. Chapman & Hall: London, 1994; pp 31-44.

23. British Geological Survey. *Groundwater Quality: Uganda;* British Geological Survey, 2001.

24. Centers for Disease Control. Arsenic: Potential for Human Exposure. Centers for Disease Control. http://www.atsdr.cdc.gov/toxprofiles/tp2-c6.pdf (accessed October 23, 2012).

# Chapter 3. Iterative Subtraction and Principal Components Analysis of the Trace Elemental Composition in Duct and Electrical Tapes

*Megan L. Mekoli; Maria K. Bock; Stanley J. Bajic; and R. Sam Houk*

Ames Laboratory-U.S. Department of Energy, Iowa State University (ISU), Ames, Iowa 50011-3020

## ABSTRACT

Tape can be used to commit a crime and is often collected as crime scene evidence. The elemental composition of tape is of forensic interest. Elemental measurements of duct and electrical tapes were taken by a nanosecond laser ablation-inductively coupled plasma-mass spectrometry. Principal component analysis (PCA) is a multivariate data reduction technique used to simplify and visualize large sets of data. The data collected was analyzed using PCA. An iterative subtraction technique is used to determine which elements contribute the most variance between differing brands of each type of tape; it's likely that some of these elements originate from bulk additives during the manufacturing process of these tapes. The adhesive and backing sides from four different brands of duct and electrical tape are analyzed using PCA and the iterative subtraction technique described. Head-to-head comparisons of these tapes are performed using Q-residual analysis. All brands of the backing and adhesive sides of duct tape were found to be distinguishable from one another to 95% confidence. Similarly, the backing side of all electrical tape brands analyzed were distinguishable from one another to 95% confidence. For the adhesive side of electrical tape, Plymouth brand electrical tape could not be distinguished from UL and Super 33 brands.

## INTRODUCTION

Duct and electrical tapes are often collected from crime scenes as evidence. These types of tapes can be used to commit a crime and may be found in bombs or from binding a victim. The composition of such a tape sample could be of forensic interest as new methods for head-to-head comparisons become available.

Searchable databases of common forms of evidence are desirable to law enforcement officials. Databases could include the trace composition of objects commonly used to commit a crime. However, the creation of a database is an exhaustive task that requires extensive time and funds. Trace analysis of tape and other materials of forensic interest (paints, glass, metals, fibers, etc.) may be accomplished by elemental analysis without quantification using statistics. Qualitative head-to-head comparison is directly matching evidence collected at a crime scene to a small set of candidate samples collected from a suspect. To prove a match using this type of analysis, forensic analysts must show how distinctive the evidence is. Statistical analysis of trace components in evidence can be used to determine the level of confidence a forensic scientist has in attributing the evidence from the crime scene to a similar candidate sample.

Traditionally, characterization and attribution of tapes as forensic evidence was accomplished by end matching [1] and microscopic evaluation methods. [2, 3, 4] Recently, trace metals and organic components in electrical tape have been measured using attenuated total reflectance-fourier transform infrared spectroscopy (ATR-FTIR), X-ray fluorescence (XRF), and middle infrared spectroscopy (MIR-IR). [5, 6, 7, 4] Goodpaster [6, 7] published a comprehensive study of electrical tapes using scanning electron microscopy with energy dispersive spectroscopy (SEM-EDS) and X-ray powder diffraction (XRPD) instrumental techniques.

Goodpaster also only measured the signals from 10 elements that could readily be seen using SEM-EDS. SEM-EDS has a detection limit of approximately 10 ppm, which is not sensitive enough for the detection of ultra-trace material. There has not been elemental analysis of duct tape in the literature to date.

Tape is very thin and prone to melting, stretching and weathering, which makes it a difficult medium to analyze. Non-destructive techniques such as SEM-EDS and XRF contain desirable attributes for analysis, however these methods lack the sensitivity to measure ultra-trace components in tape at concentrations of 10 ppb or lower. High sensitivity and the ability to rapidly analyze the trace element composition of tape sets inductively coupled plasma-mass spectrometry (ICP-MS) apart from methods used in the literature.

***Laser Ablation ICP-MS***

Dissolution of a sample of tape for analysis of trace components via ICP-MS accomplishes the sensitivity needed for ultra-trace forensic analysis, but completely destroys precious evidence. Laser ablation (LA) is a sampling technique that uses an ultraviolet laser to ablate a small amount of material from the sample surface for analysis by the ICP-MS device. LA-ICP-MS is a rapid and sensitive technique, which causes only minor sample destruction, requires no sample preparation, and is capable of measuring analytes in concentrations of 10 ppb or lower. Gray [8] was the first to combine the high sensitivity and multielement measurement capabilities of the ICP-MS with a laser, for direct sampling of solid materials. Watling became the first to use LA-ICP-MS for forensic purposes by analyzing trace elements in gold. [9] Other forensic uses of LA-ICP-MS are to match fragments

of glass, [10, 11, 12] fingerprint sapphires, [13] and compare brick stones [14] among many other areas of trace forensic science.

***Principal Components Analysis***

Multivariate statistical techniques are valuable to manage the analysis of the large sets of information produced by ICP-MS. Principal components analysis (PCA) is a statistical data reduction technique which examines variance in complex multidimensional datasets and allows for graphical visualization of groupings and trends. [10, 15] For these groupings and trends to be visualized, multiple data collections from each sample are required so as to gain a clear understanding of the content for each sample. Different runs of the same sample should have similar characteristics as each other, whereas runs of different samples may have widely varying characteristics from one sample to another.

PCA was previously used to analyze data collected from laser ablation ICP-MS measurements of glass fragments and metals. [11, 16] Goodpaster et al. have also published statistical analyses of electrical tape using PCA [6, 7] and found it was a very useful tool for analyzing multi-element data using SEM-EDS. However, they used measured signals from only 10 elements. Using PCA, Goodpaster et al. were able to distinguish 36 different classes (i.e. brands and dates of manufacture) of electrical tapes from one another.

Thus far, the analytes measured for head-to-head comparison of tapes in the literature have only been ones that are relatively abundant. Because the techniques mentioned in the literature are not sensitive enough to measure ultra-trace elements, only 10 elements that are expected to be present in all tapes have been examined. Goodpaster reported that lead content was one important distinguishing characteristic between different electrical tapes. In 2002,

lead was discontinued as a component in the production of these tapes. Therefore, tapes manufactured prior to 2002 should contain more lead. However, if the sample set is composed only of tapes manufactured prior to 2002 or after 2002, the tapes are not so easily distinguished from each other. While Goodpaster et al. were able to distinguish 36 classes of the analyzed electrical tapes from one another, perhaps more detailed information for head-to-head analysis could be gained by measurement of more elements using ICP-MS. Duct tape has not been previously examined in this way.

Ultra trace elemental analysis could help distinguish two otherwise indistinguishable samples of tape. The work described here provides a method by which elemental trace analysis may be conducted to determine which elements in tapes provide the most variability on an individual case-by-case basis.

## METHODS

### *Samples*

Duct tape is manufactured by combining a scrim (or cloth) to a polyethylene back using a poured, hot rubber adhesive. Electrical tape is manufactured by spraying hot adhesive onto a polyvinyl backing. [17, 18]

Table 1 is a list of samples that were used in this study. Exact dates of manufacture were unknown. Samples were chosen based on availability and brand popularity. Two separate rolls of 3M Super 33 electrical tape were analyzed. One was a newer roll that had been manufactured in the early 2000s and the other roll was approximately 20 years older.

Both Super 33 rolls were included in the study to determine whether tapes manufactured several years apart by the same company could be distinguished.

***Laser Ablation and ICP-MS***

The outer layer of tape still on the roll is likely contaminated, so several layers were unrolled and discarded to expose fresh tape underneath. A fresh tape sample approximately 7 cm long was cut, stretched across a large metal washer (4.4 cm outer diameter) to support the tape in the laser cell and the excess tape was trimmed off. The backing and adhesive sides were ablated in a square raster pattern through the hole in the washer, the underlying washer was not ablated. A medium resolution ($m/\Delta m = 4000$) full mass spectrum (m/z = 7 to 238 except for m/z 10 to 23, 32 to 45, 54, 79 to 82, 127, 129, 151, and 210 to 231) was acquired by a magnetic sector ICP-MS device (ELEMENT 1, Thermo Fisher Scientific Inc.), which has been described elsewhere. [19] Mass spectra were collected from seven different spots on each side of a sample of tape while ablating a square raster pattern on the surface of the sample. The interior of the ablation cell was wiped with a clean, dry kimwipe whenever the cell was opened to flip the washer or to change samples. Background signals were collected with argon flowing through the ablation cell while the laser was off.

Samples were ablated using a commercial Q-switched Nd:YAG laser (266 nm, frequency quadrupled from1064 nm, pulse length 10 ns, 9.1 mJ/pulse, CETAC LSX 500, CETAC Technologies, Omaha, NE). Laser and ICP-MS parameters may be found in Table 2. The signals at each m/z value were peak-area integrated and background subtracted. In general, signal levels corresponded to accepted isotope ratios.

***Data Analysis***

PCA was performed using the peak integrated and background subtracted signals at various m/z values with commercial software (Solo Eigenvector versions 4.0 and 6.3). To avoid biasing the data, no preprocessing such as normalizing, mean centering, or autoscaling was performed before PCA.

## RESULTS AND DISCUSSION

Figure 1 is a side-by-side comparison of peak integrated background subtracted mass spectra from two measurements of the adhesive sides of two different duct tape samples. It is difficult and time-consuming, but not impossible, to visually distinguish between the full mass spectrum for the adhesive side of Duck brand duct tape (Figure 1a) and Nashua brand duct tape (Figure 1b).

PCA is a multi-dimensional data reduction technique using the mathematics of matrices to optimize variance patterns within a large dataset. [20, 21] PCA reduces the dataset into fewer dimensions, which can be easily plotted and highlights the differences and similarities between samples. Notably, this process does not delete information from the dataset; all the original information is retained, just visually simplified.

A model is a specific set of mathematical equations that describe the reduction of one particular dataset. Different models (equations) describe different sets of data. Each equation is called a principal component. There can be multiple principal components which best describe a particular dataset. These principal components are ranked by how they best describe the differences between the samples (PC1, PC2, PC3, etc.). A score is one solution

to a principal component. Each sample will have one score for each principal component. If two samples are different, they will have two different scores for at least one principal component. Typically, one entire dataset will be reduced to two principal components that highlight the largest differences between the samples. The scores may be graphed in a coordinate plane called a scores plot to visualize how the different samples relate to one another.

A Q-residuals plot can also be used to compare how the variables (in this case, mass spectra) of each of the different brands relate to one another. A model can be created for the values of one particular subset of data (such as the mass spectra taken of different ablated spots for one particular brand of tape) within the whole dataset. The brand used as the model may be compared to all other brands. A plot of the average Q-residuals between the sample and model data represents a comparison of the averaged mass spectrum of the sample to that of the model. A large numerical Q value indicates the samples differ extensively. A 95% confidence interval may be generated from basic Gaussian statistics using the analyzed data for each separate model. The 95% confidence interval Q-value may then be plotted onto the average Q-residuals plot. Samples lying above the 95% confidence interval line are called "distinguishable from the model (to 95% confidence)" and samples lying below the 95% confidence interval are said to be "indistinguishable from the model (to 95% confidence)."

***Variance, Biplots, and the Iterative Subtraction Process***

Variance is described here as the difference between groups of sample scores compared to the span of one single group of scores. Particular variables (in this case, isotope

m/z values) that contribute the most to the overall variance between samples may be identified using a biplot and a process called iterative subtraction.

Iterative subtraction is a process of repeatedly identifying and removing the variables and their data which contribute the most variance to the model sample scores. This process is illustrated below for a dataset pertaining to the analysis of the backing side of duct tape (Figure 2). PCA makes a model ($T_0$) for that dataset ($[d_0]$) that creates the largest variance between groups of samples. In the simplest of forms, PCA can be represented by the following:

$$T_0[d_0] \qquad [1]$$

A scores plot (Figure 2) is the visual result of the model applied to that dataset. In Figure 2, the majority of the variance (99.93%) in the sample scores is captured by principal component 1 (PC 1) leaving only 0.07% of the total variance remaining. PC 2 captures the majority of the remaining variance (0.06 %). In this particular scores plot, there are distinct groups which correspond to the different brands of duct tape analyzed.

A biplot can be used to determine which variables (m/z values) contribute the most variance to the observed separation of sample groupings. [22] To create a biplot, the same model used to make the scores plot, $(T_0)$, is applied to the set of isotopic m/z variables themselves ($[M_0]$). These variables will have their own scores for each principal component, which in turn may be plotted.

$$T_0[M_0] \qquad [2]$$

The plot of $T_o[M_0]$ is overlaid onto the scores plot to form a biplot. A biplot is a visual representation showing which isotopes have the largest contribution to the variance between

samples. Isotopes which lie furthest from the origin of the biplot were most influenced by the model and therefore contribute the most to the variance between the samples in the dataset.

Figure 3 is the biplot determined from the data used in the scores plot (Figure 2) for the backing side of duct tape. The isotope furthest from the origin is m/z 27 or $^{27}$Al. In this example, $^{27}$Al is the only discernible isotope that is separated from the origin. The signal for $^{27}$Al contributes the most to the observed differences between the samples (Figure 2). Other elements could also be important, but the scale is such that only $^{27}$Al stands apart.

In order to determine which other isotopes contribute significant variance, the data corresponding to Al and the Al variable itself were removed from both the dataset and the m/z variables. Data for all isotopes of each element that contributed significant variance were eliminated to avoid confusion between minor isotopes of larger variance contribution and major isotopes of lower variance contribution. The first discernible element(s) removed are considered to be the first order variance; in this case, Al is the only element removed as the first order variance.

In Figure 3, the points for the isotopes other than $^{27}$Al cluster around the origin of the biplot. The process of applying a new model ($T_1$) to the new dataset ($d_1$) to maximize the variance between the samples, and then forming a new biplot from the remaining isotope m/z variables was repeated with the 1$^{st}$ order data and variables removed.

| | | |
|---|---|---|
| $T_1[d_1]$ | scores plot (Figure 4) | [3] |
| $T_1[M_1]$ | biplot (Figure 5) | [4] |

A second model ($T_1$) may be applied to the new dataset for these remaining elements ([$d_1$])

and a second scores plot (Figure 4) was plotted. In Figure 4, various tape samples are still separated, even though the data for the most distinctive element ($^{27}$Al) have been removed.

A second biplot (Figure 5) may be constructed by overlaying axes of the remaining isotopes onto the scores plot. The points in Figure 5 corresponding to isotopes $^{24}$Mg, $^{115}$In, $^{56}$Fe and $^{76}$Se may be discerned from the large group of points and elements. These four elements make up the second order of variance. These signals comprise most of the remaining variance, thus, the biplot process identifies the elements most responsible for the observed differences between samples. Next, the data for these 2$^{nd}$ order elements were removed.

| | | |
|---|---|---|
| $T_2[d_2]$ | scores plot (Figure 6) | [5] |
| $T_2[M_2]$ | biplot (Figure 7) | [6] |

A third scores plot (Figure 6) was created using the edited model ($T_2$) and dataset ($[d_2]$). The third scores plot in Figure 6 indicates that there is much less variance between samples as there are much fewer distinct groupings of separate samples. The third biplot (Figure 7) that was constructed shows which elements make up most of the remaining variance; $^{52}$Cr, $^{48}$Ti, $^{49}$Ti, $^{63}$Cu, and $^{65}$Cu.

This process of iteratively subtracting the data and elements which contribute the most amount of variance is repeated until the new model no longer distinguishes between the different samples. Figure 8 is a scores plot after data corresponding to elements in the first three orders of variance (Al 1$^{st}$ order; Mg, Fe, Se and In 2$^{nd}$ order; and Ti, Cr and Cu 3$^{rd}$ order) have been removed. Distinct groupings of the samples cannot be visualized in Figure 8, indicating there is little variance left between the samples. In this example, isotopic signal

data for the remaining 47 elements either does not vary from sample to sample, or corresponds to low-level noise fluctuations from the instrument.

At this point, the removed data were combined into a final dataset [$d_f$] upon which a final model ($T_f$) was applied. Data for the m/z values other than these identified in the 1$^{st}$ – 3$^{rd}$ orders were not present in [$d_f$].

$T_f[d_f]$ final scores plot (Figure 9) [7]

The final scores plot in Figure 9 is very similar to the initial scores plot (Figure 2), indicating that only the data from elements contained in the first three orders of variance were necessary to accurately compare this set of samples.

This iterative subtraction technique was used to determine which elements contribute most to the observed variance between samples of two kinds of the tape (duct and electrical), both adhesive and backing sides. Elements were removed and grouped in order of decreasing contribution to the variance between the brands until the various samples could no longer be distinguished. In the case of all tapes analyzed, only three consecutive orders of element classification using scores plots and biplots were necessary.

***Duct Tape, Backing Side***

Figure 9 is the final scores plot ($T_f[d_f]$) for measurements taken from the backing side of four separate brands of duct tape after elements in the 1$^{st}$, 2$^{nd}$, and 3$^{rd}$ orders of variance were identified from the biplot process. The separations in scores of one group from those of members of a different group indicate that the samples within the first group can be distinguished from the second group based on the acquired mass spectra. Points on the scores plot which appear to overlap indicate the samples are not distinguishable from one another

based upon the acquired mass spectra.

Biplots were constructed from the scores data and the iterative subtraction technique was applied. The elements found in the orders of variance table (Table 3) correspond to the elements which contribute the most variance between the different brands. Aluminum is a bulk additive in duct tape to achieve the silver hue of the backing. [17] If Al is present in all duct tapes, it is not expected to be distinctive. However, the high variance in Al abundance between different duct tape brands indicates that different manufacturers add Al in widely varying amounts to give the tape silver hues that are distinct from other manufacturers' products. Al is also typically added to the adhesive side of duct tapes as kaolinite ($Al_2Si_2O_5(OH)_4$) during the manufacturing process to add volume, reinforce the rubber adhesive or add color. [17] Magnesium likely comes from talc ($Mg_3Si_4O_{10}(OH)_2$), which is added to duct tapes for strength and to make them water repellent. Titanium likely originates from $TiO_2$, which may leak into the backing side from the adhesive side, as it is a common component in duct tape adhesives. [17] Iron could be present from tape contact with metal parts during the manufacturing and packaging process or may have been an inorganic additive by the manufacturers. The origins of In and Se are unclear.

Figure 10 is the average Q-residuals plot derived from the scores after the three orders of variance (Table 3) were combined. The separation in the variables is almost identical to those of the scores plot constructed prior to the iterative subtraction technique (data not shown). Scores for the subtracted elements of all brands were compared to those of the model brand. All average Q-values for each sample compared to each model are above the 95% confidence interval. The average Q-residuals plot in Figure 10 indicates that the backing sides of all brands of duct tape are distinguishable from one another to 95% confidence.

***Duct Tape, Adhesive Side***

Figure 11 is the scores plot for the adhesive side of duct tape using data only for elements from the first three orders of variance. This plot is similar to the original scores plot (not shown) that includes all data taken for all variables. Table 4 lists the orders for the elements; Al, Fe, Cu, Se, and In contribute the most variance between the brands on the adhesive side of duct tape. Again, Al is included as an element which contributes much variance in the first order. Large amounts of Al on the adhesive could be contamination from contact with the backing side while the tape was rolled up, or from unintentional sampling of the backing side while ablating the adhesive side. Due to the thinness of the adhesive layer, unintentional sampling of the backing side while ablating the adhesive side or vice versa could have been possible even though it was not specifically observed.

There are distinct groupings of ablated spots associated with each of the four brands in the scores plot in Figure 11. These scores were compared to one another using an average Q-residuals plot (Figure 12). In the Q-residuals plot (Figure 12), all points lie above the 95% confidence interval indicating all brands are distinguishable from one another to 95% confidence.

***Electrical Tape, Backing Side***

Figure 13 is the scores plot for the backing sides of electrical tape using only those elements identified by the iterative subtraction technique. Table 5 lists elements contained in the first three orders of variance for the backing side of electrical tape. From Table 5, Pb and Sb contribute the most variance between the brands. Pb was once used in electrical tape as plasticizer. [17]

The amount of Sb detected could be from antimony oxide ($Sb_2O_3$), which is a common inorganic additive to electrical tape backing. [17] Titanium is another common inorganic additive to electrical tapes, which can be incorporated as titanium oxide ($TiO_2$); [17] however, its abundance was found to vary less than Sb and Pb between the brands analyzed.

The orders of variance listed in Table 5 indicate that ultra-trace elements such as Mo and Bi contribute to the variance in the scores plots. These elements are easily recognizable, vary between the brands, and could be transferred to tape by roller contact during the manufacturing process. Molybdenum and Bi have not been measured in electrical tapes in previous studies (such as those from Goodpaster [6] and Mehltretter [4]) possibly because they are not known additives in the bulk manufacturing process. This information regarding Bi and Mo content could have otherwise been overlooked were it not for the sensitivity and elemental coverage of ICP-MS and the large data management of PCA combined with the iterative subtraction technique.

These additives were found to be three of the handful of elements which contributed the most to the variance between different brands for the backing side of electrical tape. Each manufacturer of electrical tape could have its own "recipe" of additives, making brand comparison easier.

From Figure 14, the average Q-residual values for all brands fall above the 95% confidence value when compared to models created from each brand. This indicates all brands of the backing side of electrical tape analyzed here are distinguishable from one another to 95% confidence.

***Electrical Tape, Adhesive Side***

Figure 15 is the scores plot for the adhesive side of electrical tape. This side of electrical tape is usually a thin layer of adhesive that is unevenly painted or sprayed onto the backing. This layer is so thin that is difficult to ablate without sampling the backing side as well. Thus, results from the adhesive side are likely to contain elements from both the adhesive and backing sides.

Figure 16 is the average Q-residuals plot for each brand of tape. When Plymouth brand tape is used as the model, that brand cannot be distinguished from UL and Super 33 to 95% confidence.

The corresponding scores plot for these four brands (Figure 15) shows why. At first glance, the scores for each brand of tape seem to be easily distinguishable from one another. However, the scores for Plymouth brand (blue squares) are well spread out, pushing the 95% confidence interval value further out to encompass the points of both UL and Super 33 scores.

When Super 33 is used as the model, the Q-residuals values for the other brands (Old Super 33, UL, and even Plymouth) are distinguishable to 95% confidence. The scores for Super 33 brand tapes cluster very close in one region of the scores plot, making the 95% confidence interval very small. Scores from other brands do not fall within the 95% confidence interval for Super 33 brand tapes, even though they are in close proximity. The scores for UL brand behave similar to those of Super 33. Although the average Q-residual values indicate that UL, Super 33 and Plymouth brands are indistinguishable from one another to 95% confidence, Figure 16 does show that Super 33, Old Super 33 and UL brands are distinguishable from one another to 95% confidence. These results highlight the

importance of using different sets of results as the model to gain a full understanding of all brands.

The iterative subtraction of elements contributing the most variance to the backing side of these brands was performed and elements corresponding to the first three orders of variance may be found in Table 6. Given the nature of the adhesive side application and the difficulty in analyzing solely the adhesive side, it is difficult to make any conclusions regarding those elements which contribute the most variance to the adhesive side only.

## CONCLUSION

An iterative subtraction technique was used to identify the elements that contributed the most variance to the distinction between different brands of tape in conjunction with a multivariate statistical data analysis technique such as PCA. A successful head-to-head elemental analysis of the backing and adhesive sides of duct tape was demonstrated using iterative subtraction applied to PCA. This method was applied to both the backing and adhesive sides of duct tape. All brands of duct tape analyzed here were distinguishable from one another.

From Tables 3 and 4, the Al signal is captured in the 1$^{st}$ order variance in both the adhesive and backing sides of duct tapes. This indicates that the amount of Al varies greatly in duct tapes. The level of Al in could be used as a quantitative diagnostic to rapidly differentiate between different brands of duct tape.

The method described here was also applied to both sides of electrical tape. The technique was only successful at distinguishing *all* brands from one another for the backing

side. However, analysis for the adhesive side highlighted the importance of varying the set of results that are used as the model. Additionally, it is likely that all brands could not be distinguished from one another for the adhesive side of electrical tape due to difficulties sampling only the adhesive. The very thin, uneven nature of the adhesive side on electrical tape could have been a limiting factor of accurately analyzing this side.

PCA in conjunction with iterative subtraction to determine elemental variance contribution has been shown here to be useful in distinguishing between different brands of tapes. This method has been shown to identify important elements that are not immediately obvious from mass spectra these distinctive elements are not necessarily the most abundant ones. The process provides extra information of potential forensic value.

The use of biplots in addition to PCA may serve as an additional tool for forensic scientists when performing trace elemental analysis of tapes. The method used here could also be applied to other forms of evidence. Similar trace elemental analysis studies of other common forms of evidence collected at crime scenes such as paints, and glass could be useful to forensic scientists.

Similarly, the merits of femtosecond laser ablation as a sampling technique for ICP-MS over that of nanosecond laser ablation have been shown to decrease fractionation and melting effects caused by sample heating. [22] Femtosecond ablation could be advantageous to tape, which is very thin and prone to melting. Utilization of such a laser with the technique described here could yield additional important tools for accurate analysis.

## TABLES

**Table 3** List of pressure sensitive tapes analyzed

| Tape | Identifier | Manufacturer |
|---|---|---|
| Duct | | |
| | Duck | ShurTech Brands, LLC |
| | 3M | 3M Company |
| | Nashua | Tyco Adhesives |
| | Staples | Staples, Inc. |
| Electrical | | |
| | Super 33 | 3M Company |
| | Old Super 33 | 3M Company (manufactured before 2000) |
| | Plymouth | Plymouth Rubber Co. |
| | UL | Ningbo Universal Tools Co, LTD |

**Table 4** Instrument and laser parameters for the analysis of duct and electrical tapes

| | |
|---|---|
| ICP-MS Instrument | ELEMENT 1 (Thermo, inc.) |
| nsLaser used for ablation of brand comparison | CETAC LSX 500 Nd:YAG |
| Operational wavelength | 266 nm |
| Laser energy | 12.1 mJ $pulse^{-1}$ |
| Frequency | 20 Hz |
| Spot size | 100 µm |
| Raster speed | 350 µm $sec^{-1}$ |
| Sampler and skimmer cones | Ni, H configuration (Thermo, inc.) |
| Sample gas | 1.06 L Ar $min^{-1}$ |
| RF Power | 1150 W |
| Outer/auxiliary gas stream | 16.00/1.16 L Ar $min^{-1}$ |
| Torch position, ion optics | Optimized for maximum sensitivity and stability |
| Scan mode<br>dwell/settling time | Peak jump, 10 points per mass, 10 ms dwell time,<br>2.1 ms settling time |
| Acquisition | |
| Runs/passes | 3 runs/1 pass |
| Elements measured (medium resolution) | Li, Mg, Al, P, Sc, Ti, V, Cr, Mn, Fe, Co, Ni, Cu, Zn, Ga, Ge, As, Se, Rb, Sr, Y, Zr, Nb, Mo, Ru, Rh, Pd, Ag, Cd, In, Sn, Sb, Te, Cs, Ba, La, Ce, Pr, Nd, Gd, Ho, Hf, Ta, W, Re, Os, Ir, Pt, Au, Hg, Tl, Pb, Bi, Th, U |

**Table 5** Variance contribution of isotopes to the model for the backing side of duct tape. Signals for these isotopes were used to create the scores plot in Figure 9.

| Order of Variance | Isotopes |
|---|---|
| 1st | $^{27}Al$ |
| 2nd | $^{24}Mg$, $^{56}Fe$, $^{76}Se$, $^{78}Se$, $^{113}In$, $^{115}In$ |
| 3rd | $^{46}Ti$, $^{47}Ti$, $^{48}Ti$, $^{49}Ti$, $^{52}Cr$, $^{53}Cr$, $^{63}Cu$, $^{65}Cu$ |

**Table 4** Variance contribution of elements to the model for the adhesive side of duct tape. Signals for these isotopes were used to create the scores plot in Figure 11.

| Order of Variance | Isotopes |
|---|---|
| 1st | $^{27}Al$, $^{56}Fe$, $^{63}Cu$, $^{65}Cu$, $^{76}Se$, $^{78}Se$, $^{113}In$, $^{115}In$ |
| 2nd | $^{24}Mg$, $^{46}Ti$, $^{47}Ti$, $^{48}Ti$, $^{49}Ti$ |
| 3rd | $^{31}P$, $^{55}Mn$, $^{52}Cr$, $^{53}Cr$, $^{86}Sr$, $^{88}Sr$ |

**Table 5** Variance contribution of elements to the model for the backing side of electrical tape. Signals for these isotopes were used to create the scores plot in Figure 13.

| Order of Variance | Isotopes |
|---|---|
| 1st | $^{121}$Sb, $^{123}$Sb, $^{206}$Pb, $^{207}$Pb, $^{208}$Pb |
| 2nd | $^{46}$Ti, $^{47}$Ti, $^{48}$Ti, $^{49}$Ti, $^{92}$Mo, $^{95}$Mo, $^{96}$Mo, $^{98}$Mo, $^{135}$Ba, $^{137}$Ba |
| 3rd | $^{56}$Fe, $^{66}$Zn, $^{68}$Zn, $^{76}$Se, $^{78}$Se, $^{86}$Sr, $^{88}$Sr, $^{209}$Bi |

**Table 6** Variance contribution of elements to the model for the adhesive side of electrical tape. Signals for these isotopes were used to create the scores plot in Figure 15.

| Order of Variance | Isotopes |
|---|---|
| 1st | $^{46}$Ti, $^{47}$Ti, $^{48}$Ti, $^{49}$Ti, $^{56}$Fe, $^{121}$Sb, $^{123}$Sb, $^{206}$Pb, $^{207}$Pb, $^{208}$Pb |
| 2nd | $^{31}$P, $^{66}$Zn, $^{68}$Zn, $^{76}$Se, $^{78}$Se, $^{135}$Ba, $^{137}$Ba, $^{140}$Ce, $^{142}$Ce |
| 3rd | $^{51}$V, $^{52}$Cr, $^{53}$Cr, $^{63}$Cu, $^{65}$Cu, Zr, $^{86}$Sr, $^{88}$Sr, $^{118}$Sn, $^{120}$Sn, $^{139}$La, $^{209}$Bi |

**FIGURES**

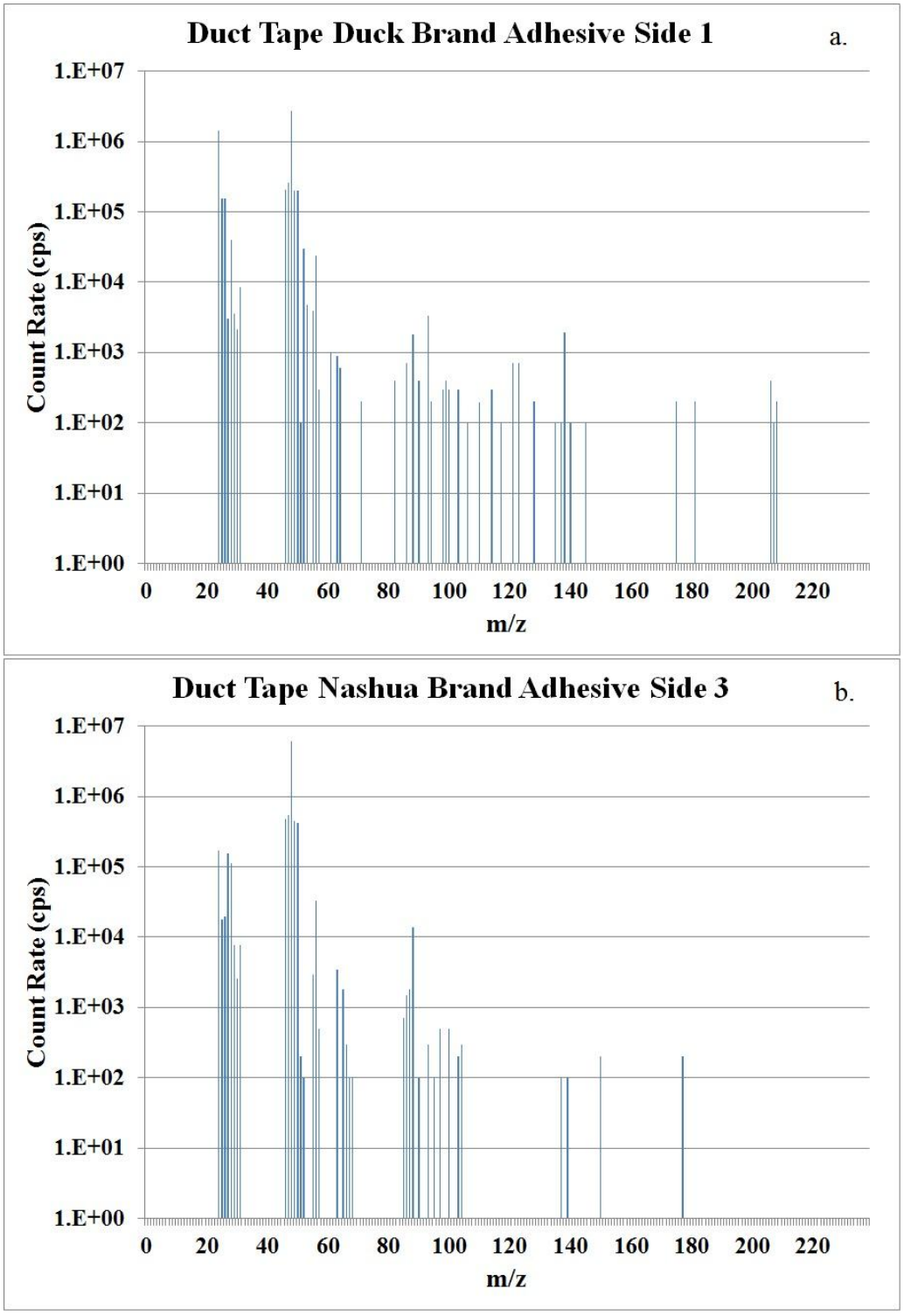


**Figure 3** Mass spectra for one adhesive side sampling for two brands of duct tape. a. corresponds to the spectrum measured for the first sampling of Duck brand duct tape and b. corresponds to the spectrum measured for the third sampling of Nashua brand duct tape.

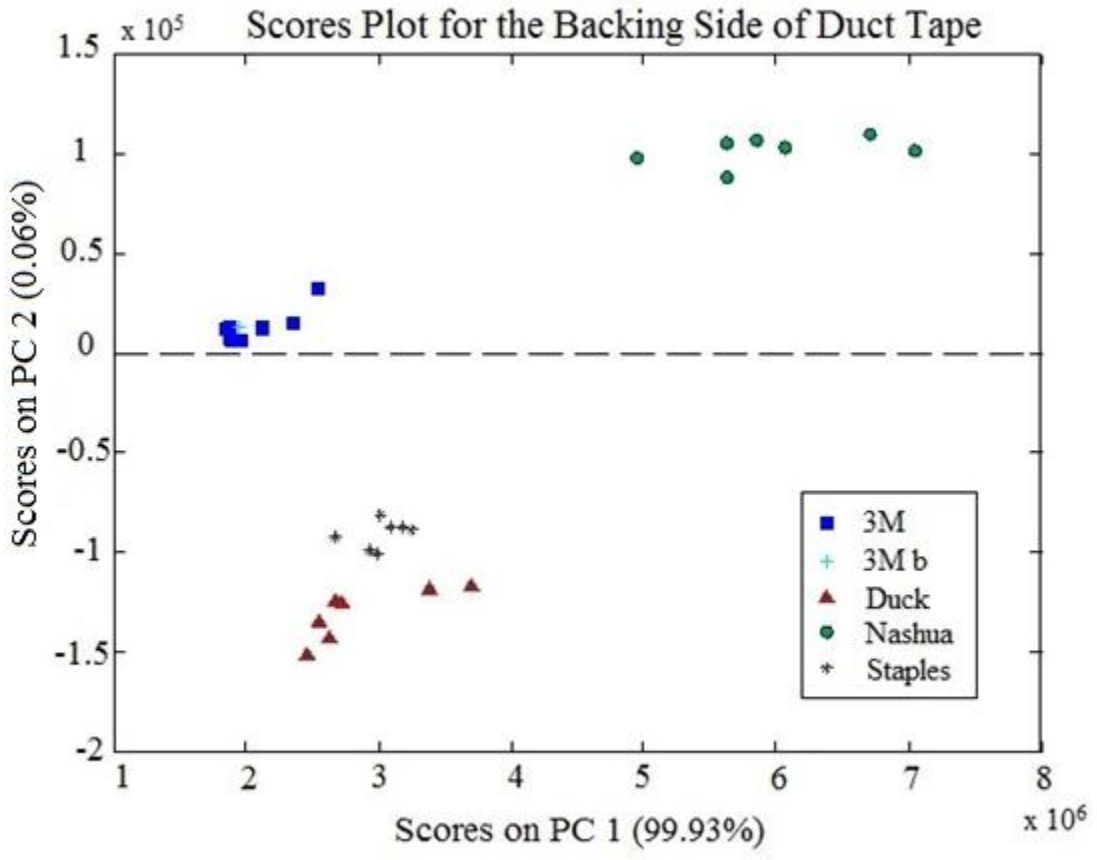


**Figure 4** Scores plot for the backing side of duct tape. All data collected corresponding to all elements measured was used to create the scores plot shown above. The numbers in the parentheses indicate the amount of variance captured in the principal component. The model was based on all data collected for all elements measured. The point labeled "3M b" was an extra point analyzed at the end of the experiment to monitor instrumental drift.

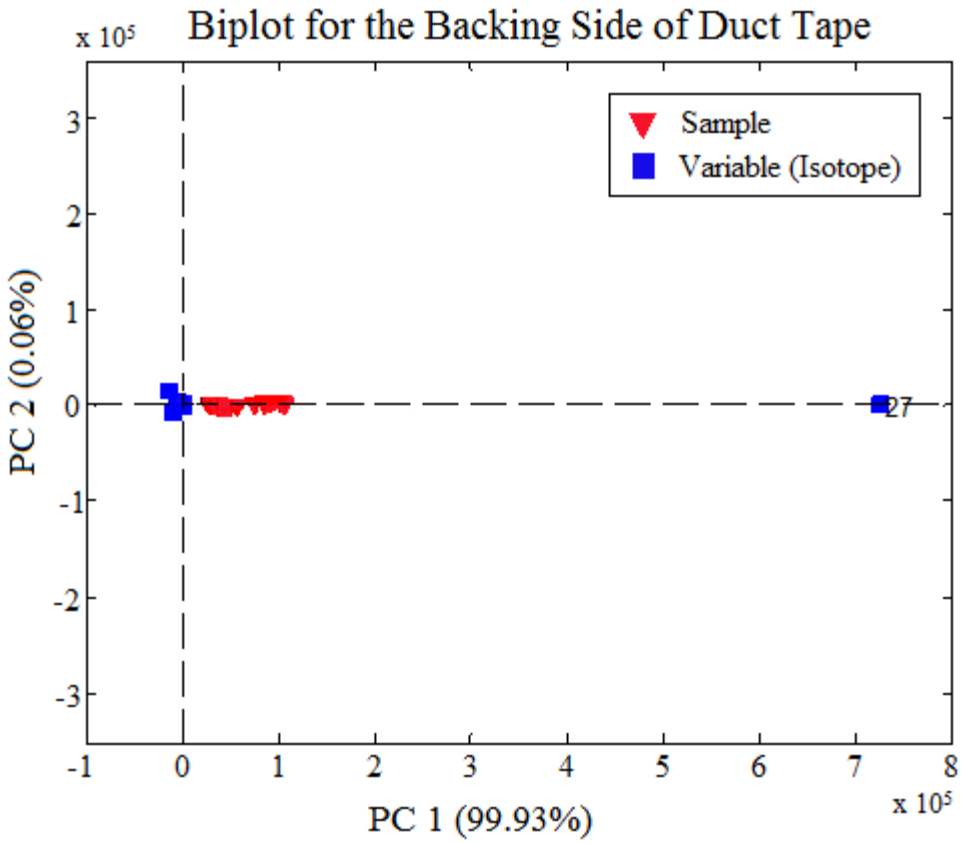


**Figure 5** Biplot for the backing side of duct tape showing the 1st order of variance. This plot was achieved by overlaying the variable axes onto the scores plot found in Figure 2. Variables (in this case isotope masses, blue squares) which contribute the most variance to the separation of the samples (red triangles) lie farther away from the origin. Isotope mass 27, corresponding to Al, contributes the most variance to the sample scores.

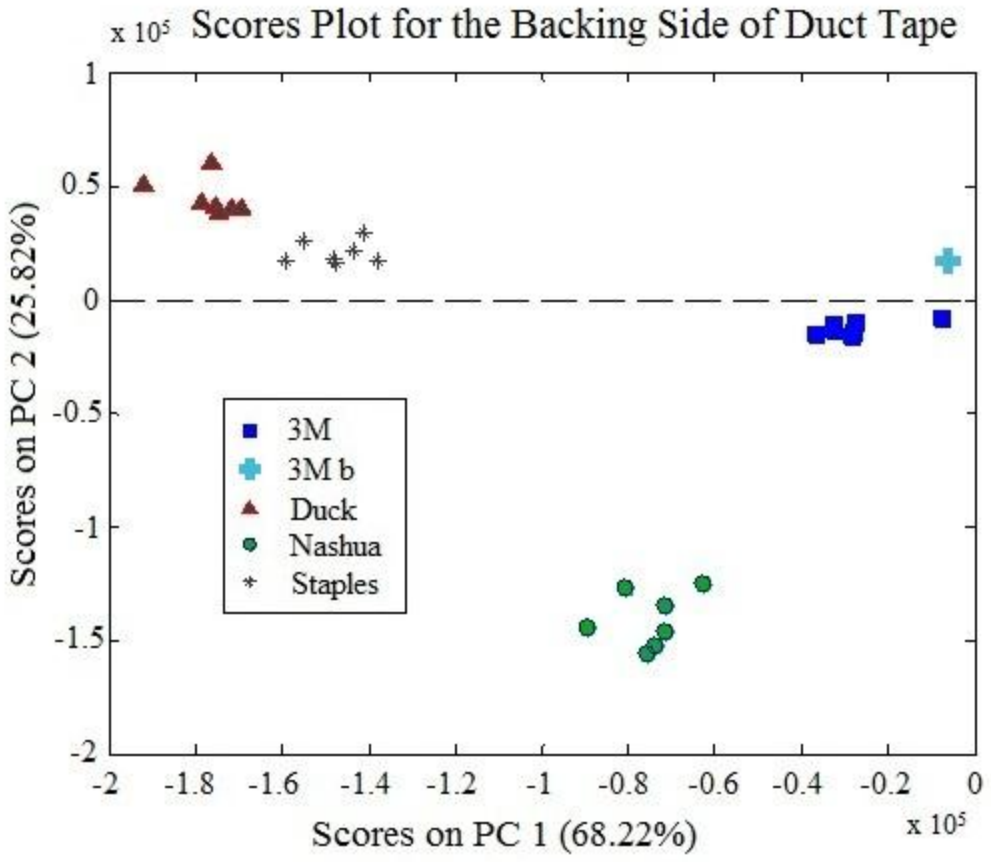


**Figure 6** Scores plot for the backing side of duct tape after the element(s) corresponding to first order variance has been removed.

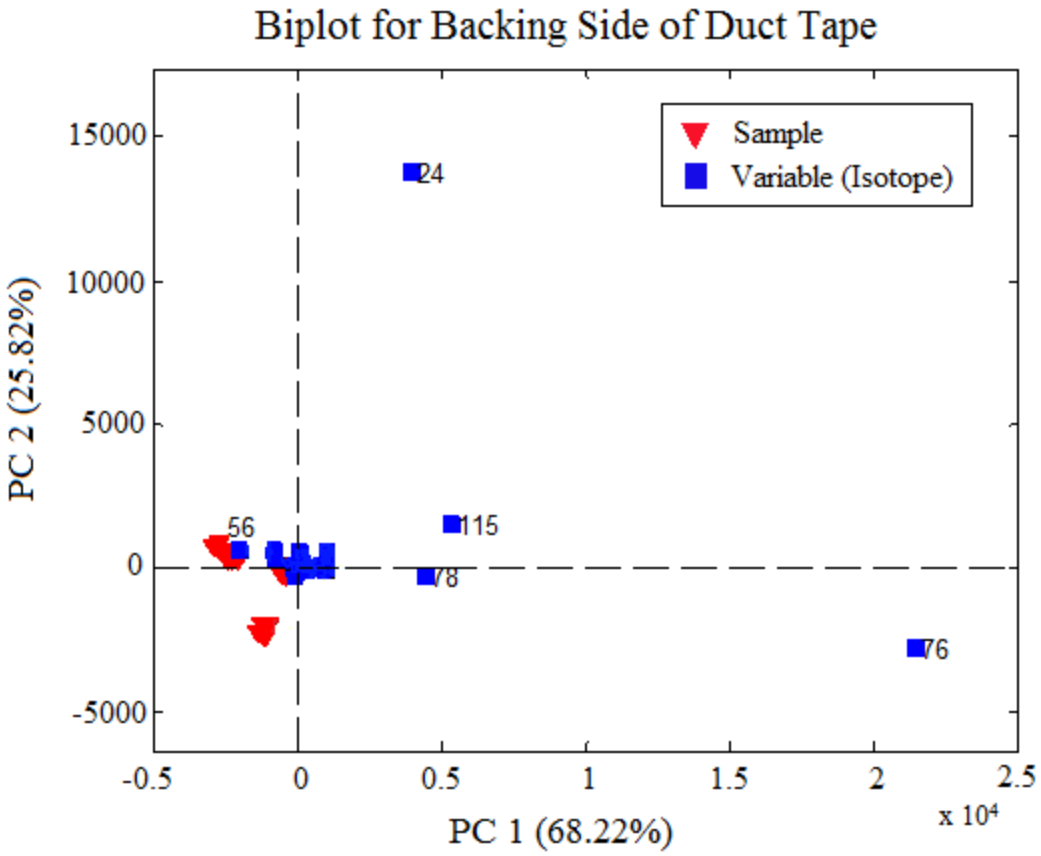


**Figure 7** Biplot showing the 2nd order variance for the backing side of duct tape. Variables (isotope masses, blue squares) contributing the most variance to the sample scores (red triangles) are labeled above. Isotope mass 24 corresponds to Mg, 115 corresponds to In, 76 and 78 correspond to Se, and 56 corresponds to Fe.

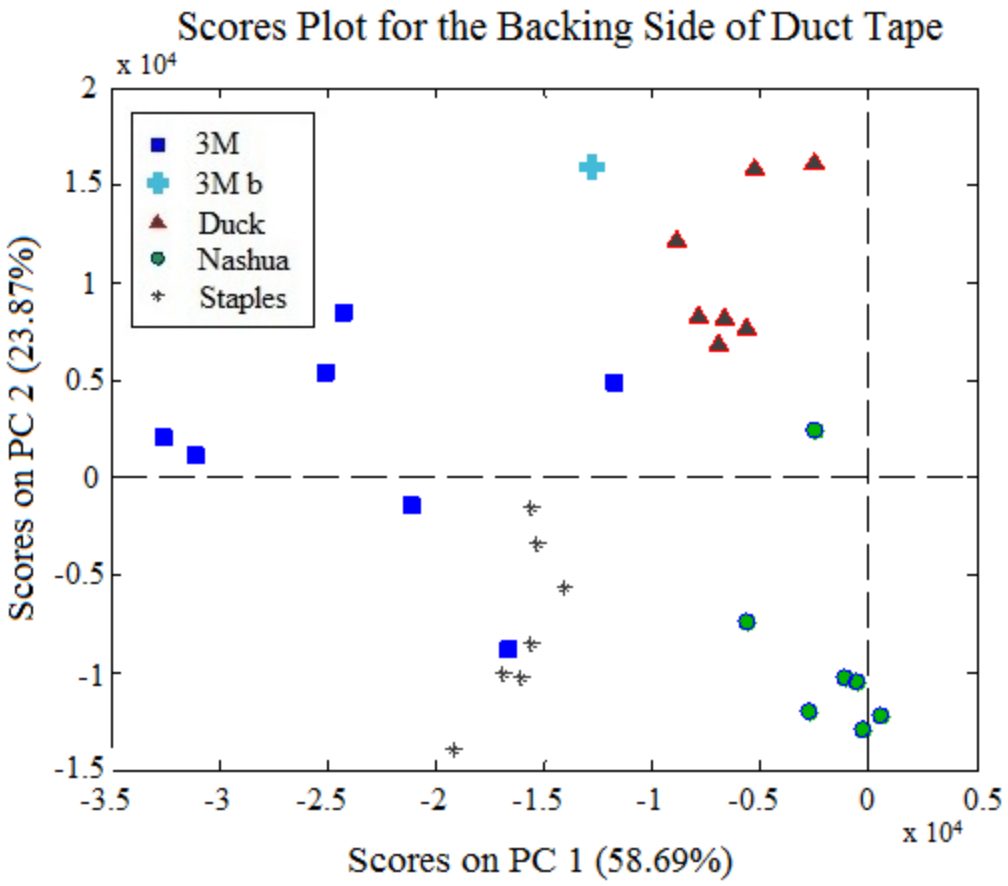


**Figure 8** Scores plot with data corresponding to the 1st and 2nd orders of variance removed for the backing side of duct tape.

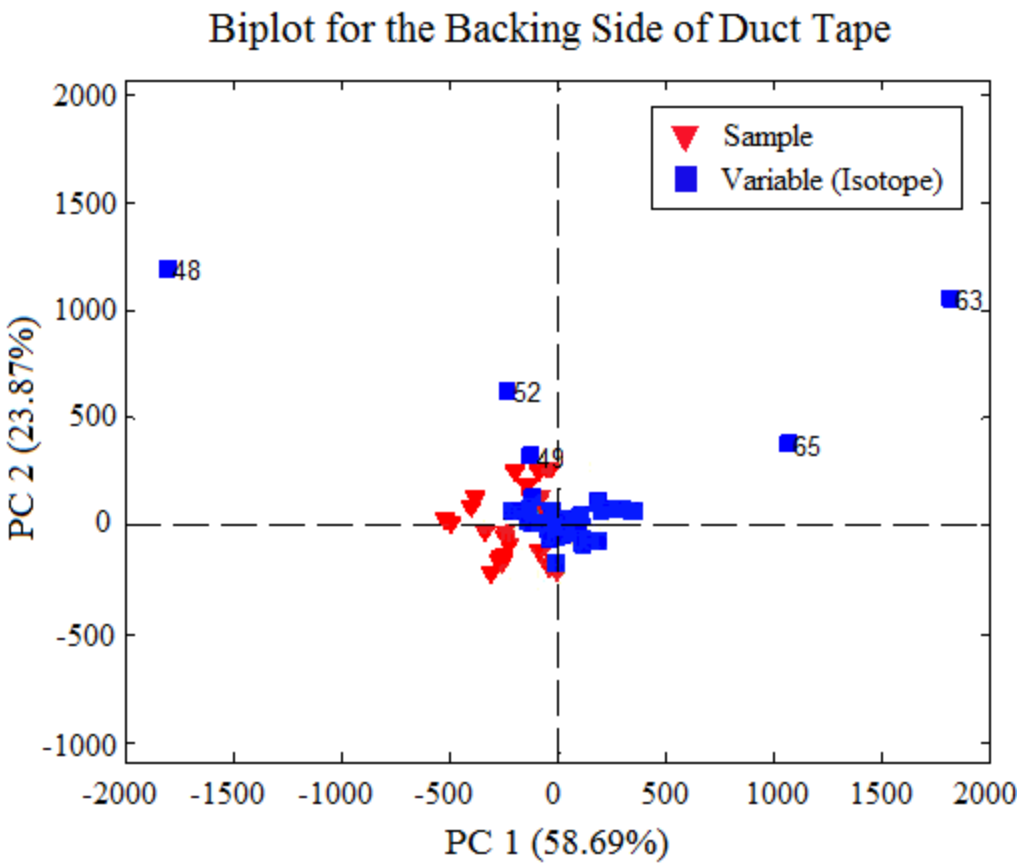


**Figure 9** Biplot showing the 3nd order variance for the backing side of duct tape. Variables (isotope masses, blue squares) contributing the most variance to the sample scores (red triangles) are labeled above. Isotope mass 48 corresponds to Ti, 52 corresponds to Cr, and both 63 and 65 correspond to Cu.

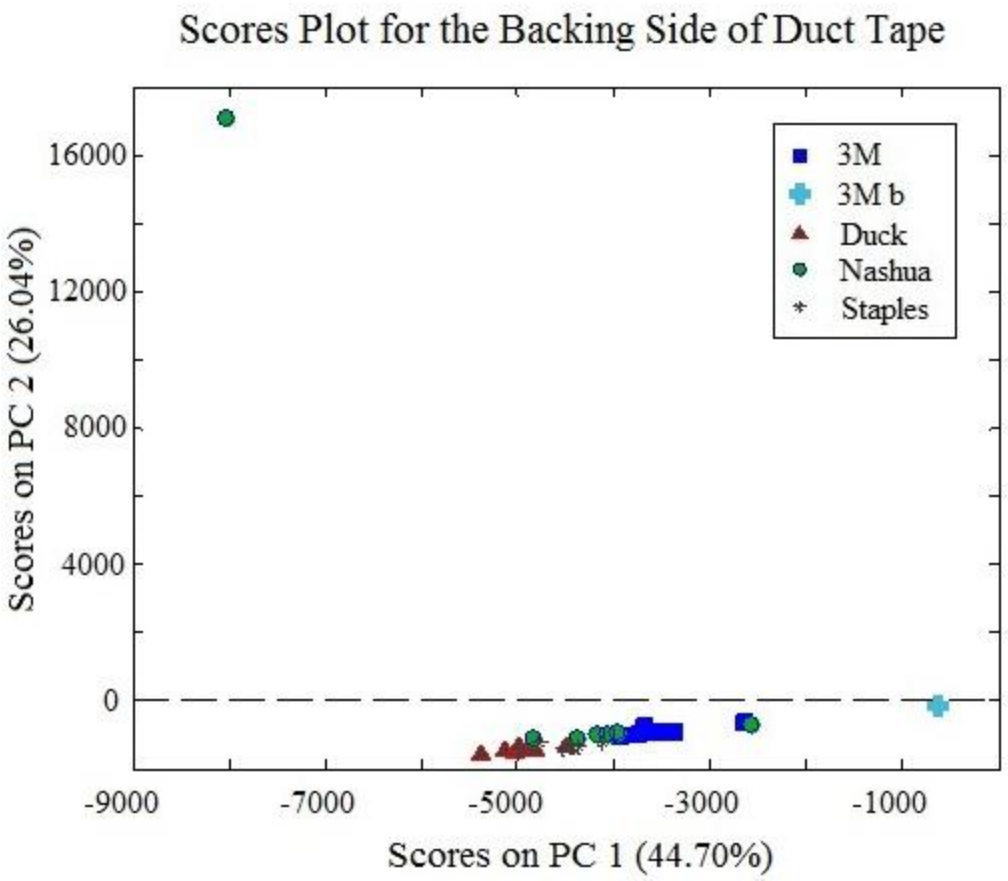


**Figure 10** Scores plot for the backing side of duct tape after data for elements corresponding to the first three orders of variance have been removed.

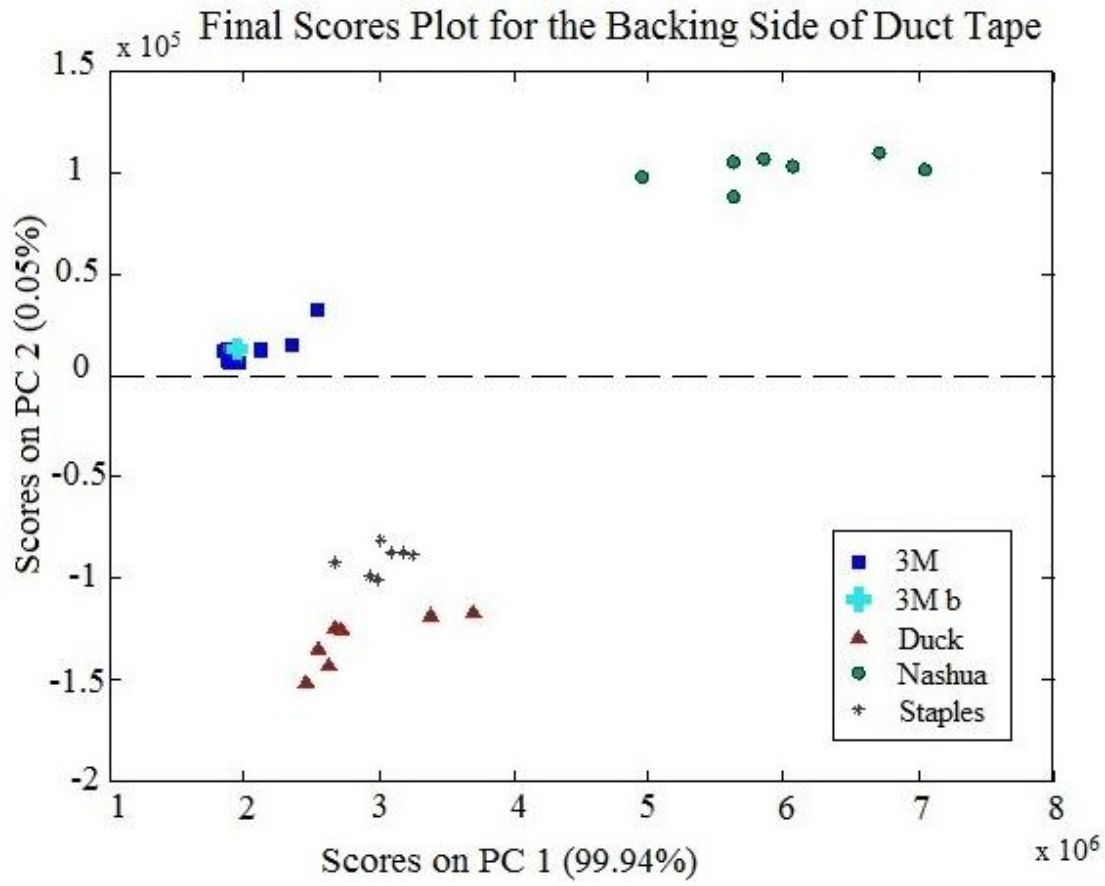


**Figure 9** Final scores plot for the backing side of duct tape using data only from elements in the 1st, 2nd and 3rd orders of variance.

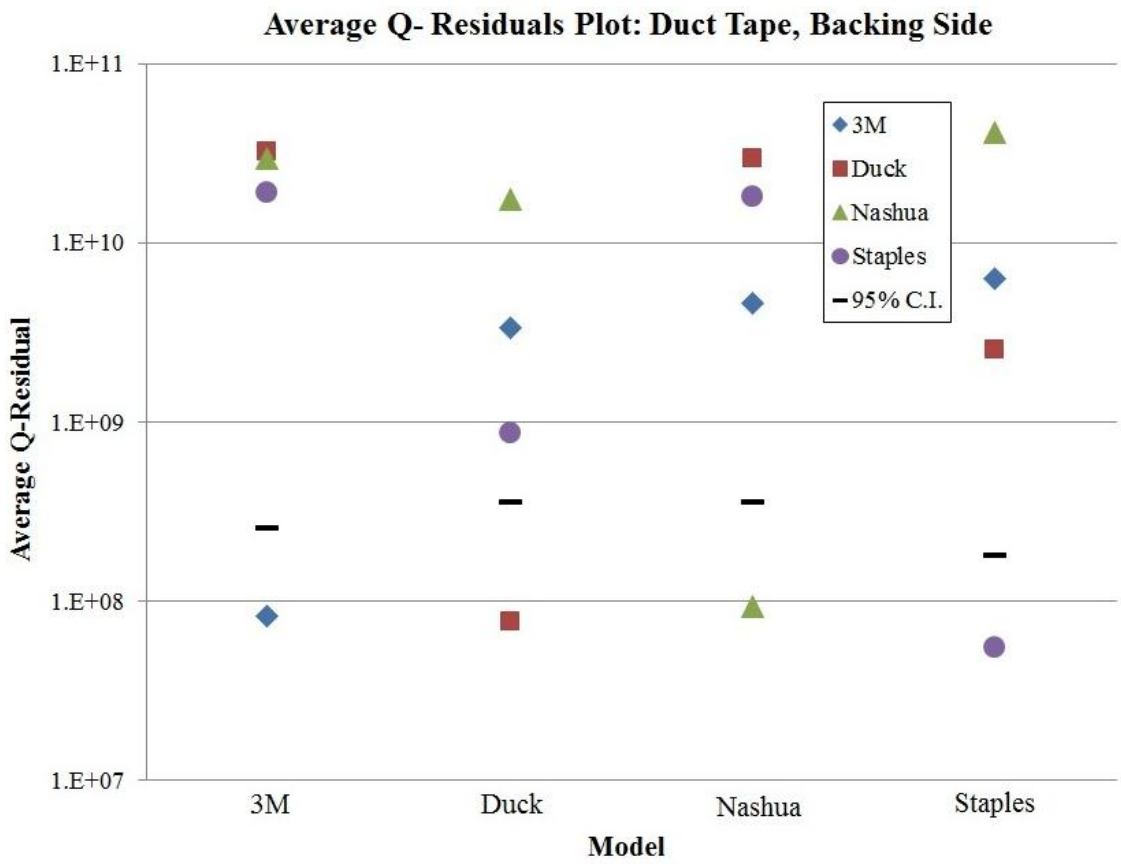


**Figure 10** Average Q-residuals plot for the backing side of duct tape. The black line denotes the 95% confidence interval for each model.

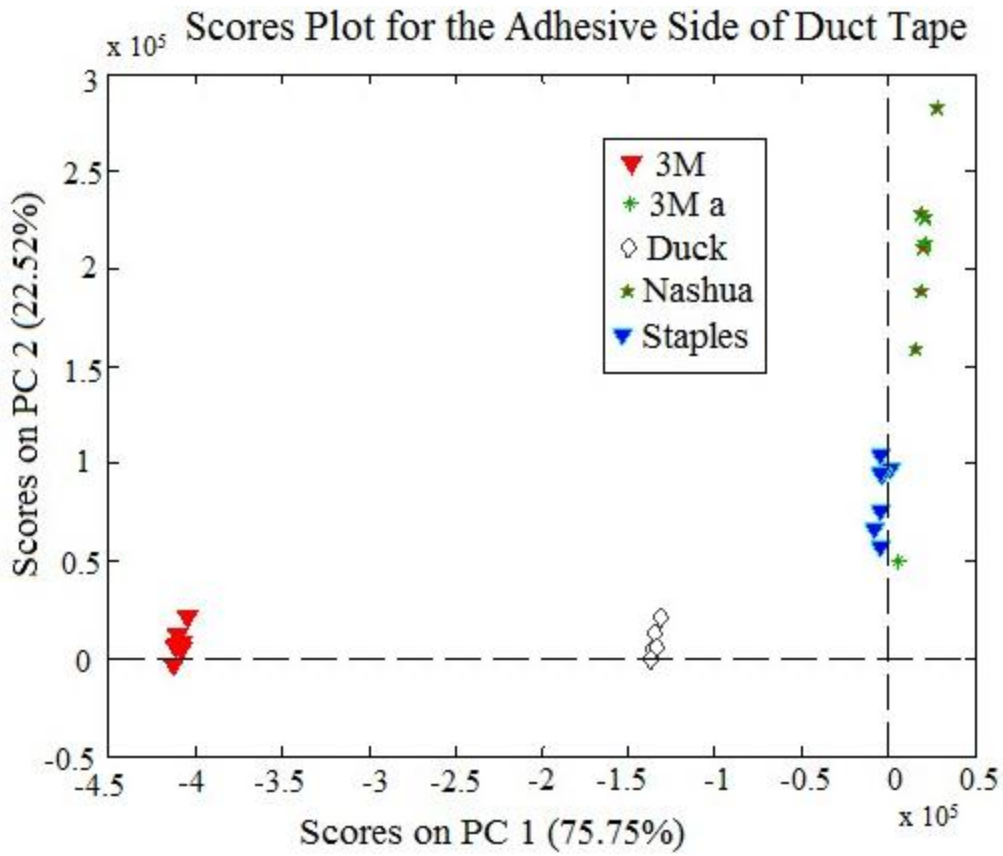


**Figure 11** Scores plot for the adhesive side of duct tape. The numbers in the parentheses indicate the amount of variance captured by each principal component. The model was based on elements contained in the first three orders of variance. The point labeled "3M a" was an extra point analyzed at the end of the experiment to monitor instrumental drift.

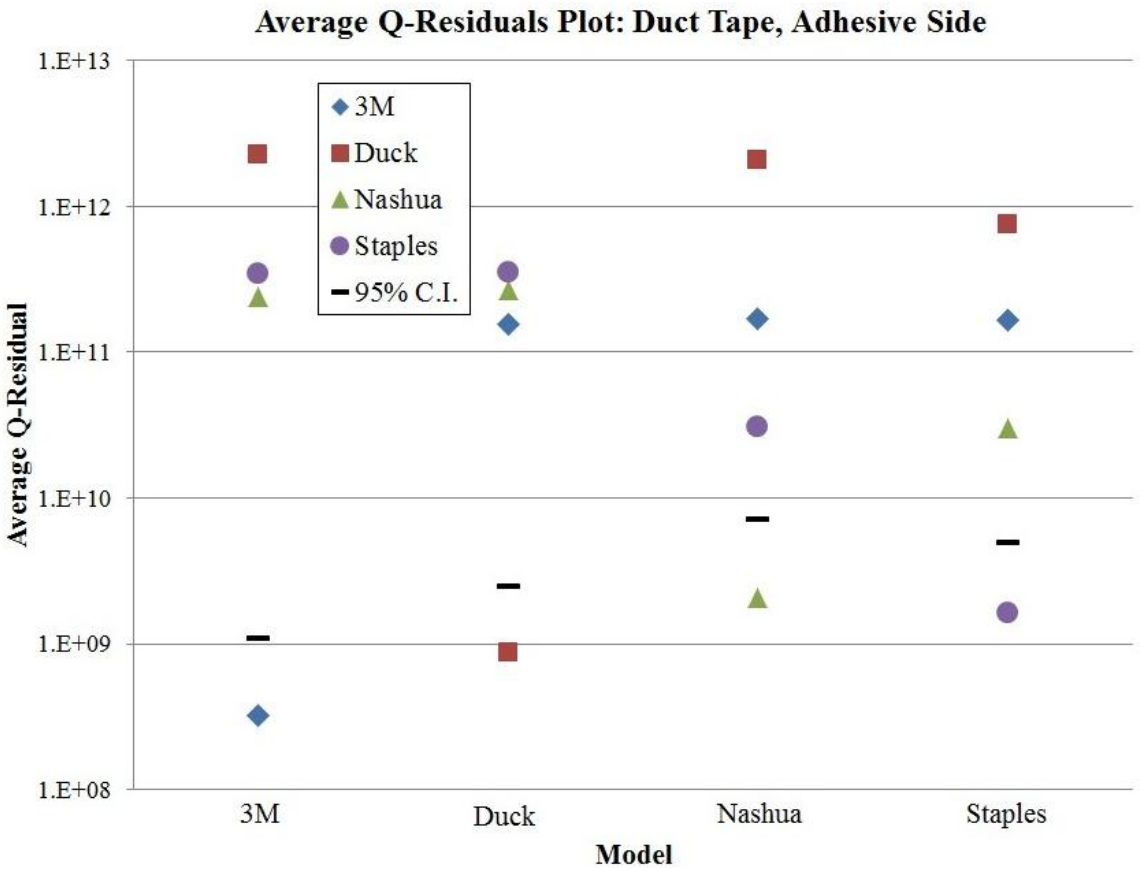


**Figure 12** Average Q-residuals plot for the adhesive side of duct tape. The black line denotes the 95% confidence interval for each model.

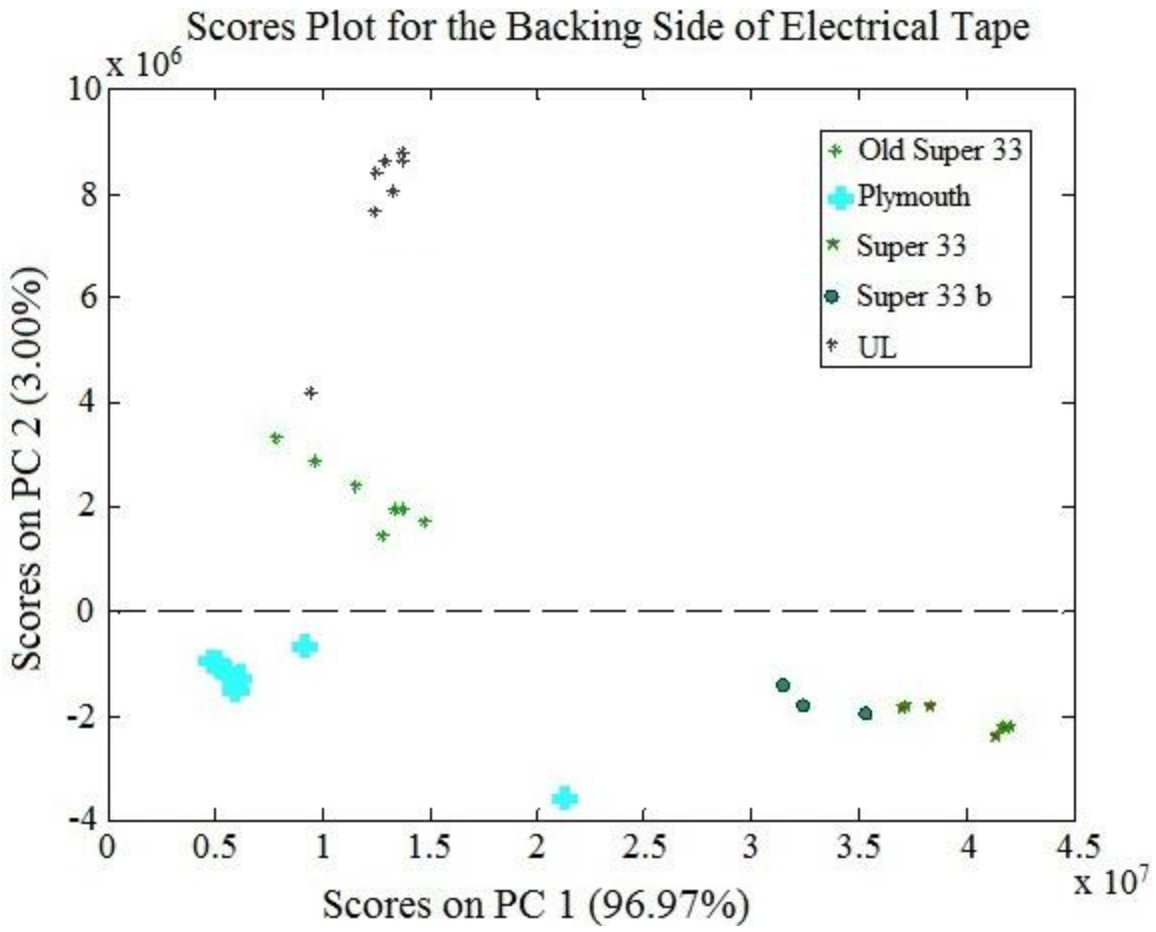


**Figure 13** Scores plot for the backing side of electrical tape. The numbers in the parentheses indicate the amount of variance captured in the principal component. The model was based on elements contained in the first three orders of variance (Table 5).

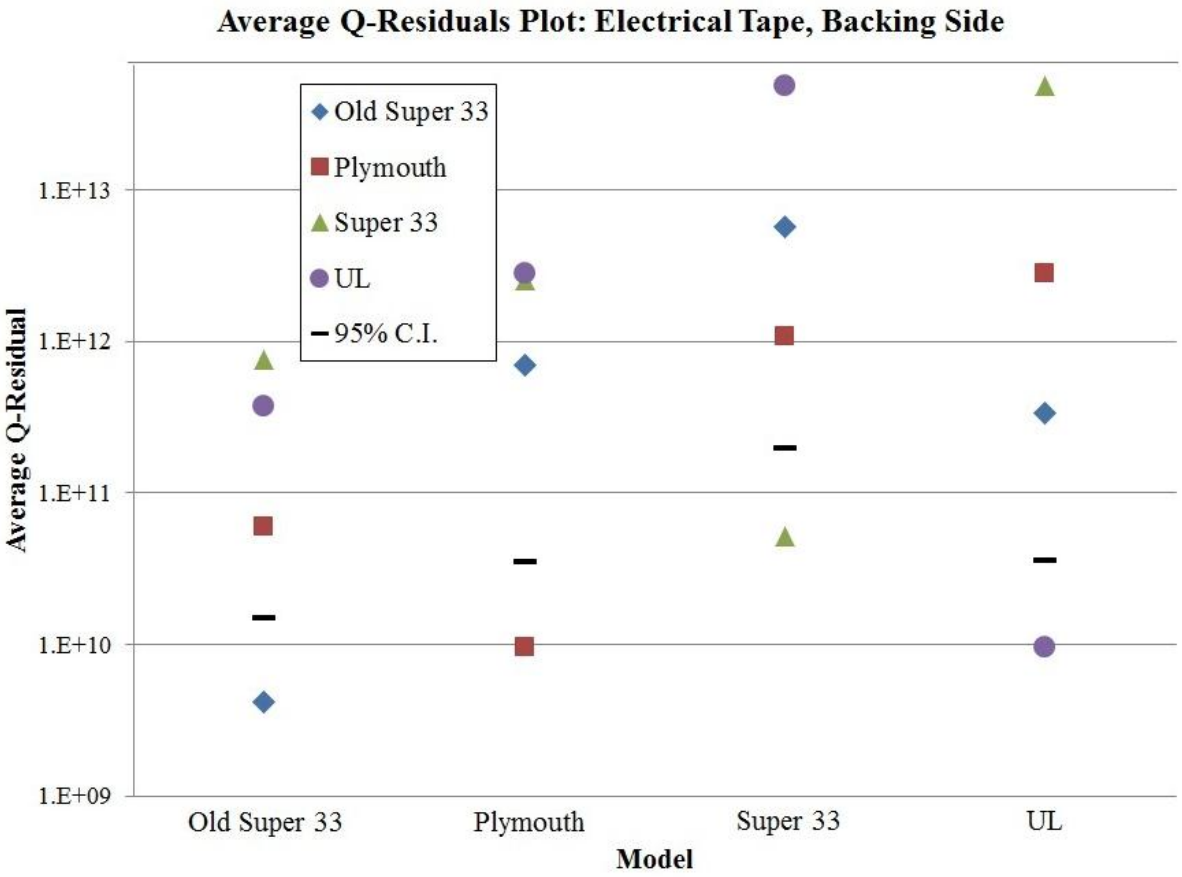


**Figure 14** Average Q-residuals plot for the backing side of electrical tape. The black line denotes the 95% confidence interval for each model.

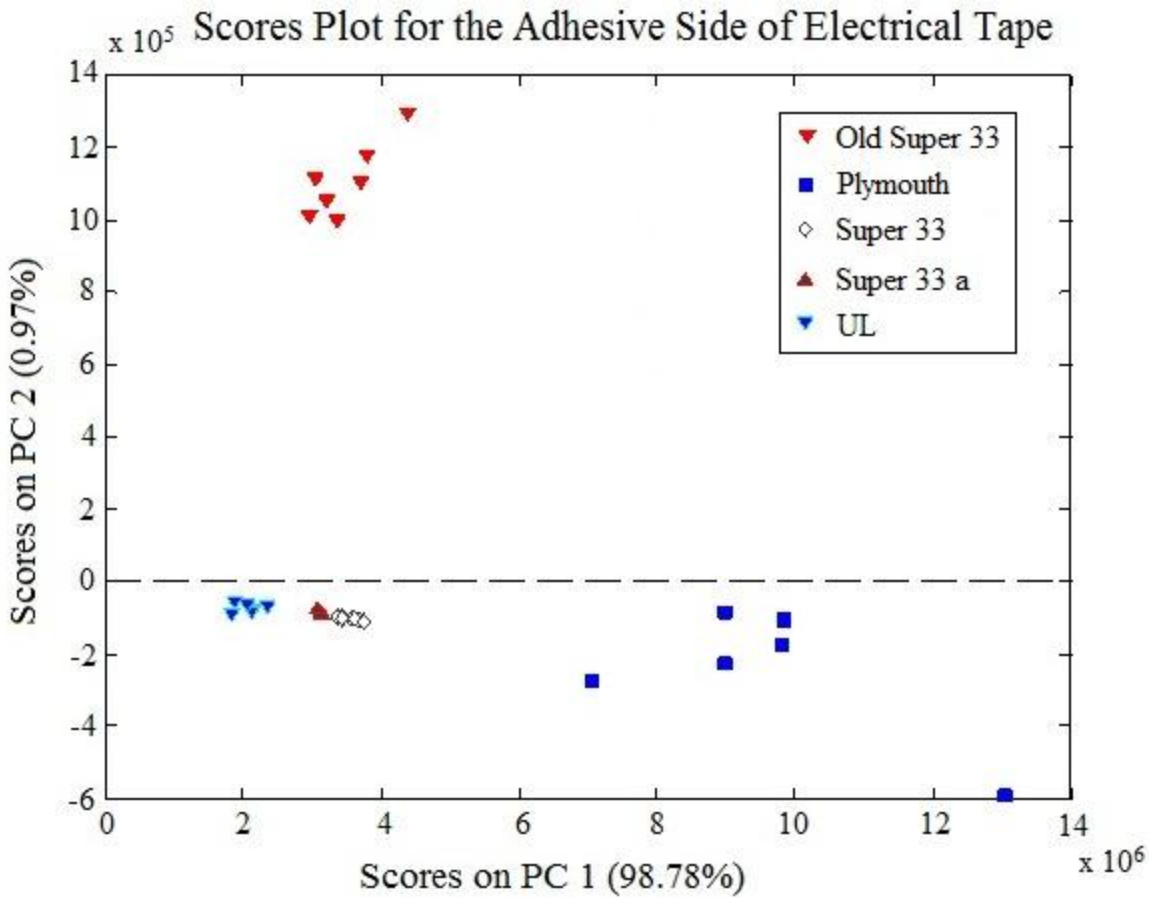


**Figure 15** Scores plot for the adhesive side of electrical tape. The numbers in the parentheses indicate the amount of variance captured in the principal component. The model was based on elements contained in the first three orders of variance.

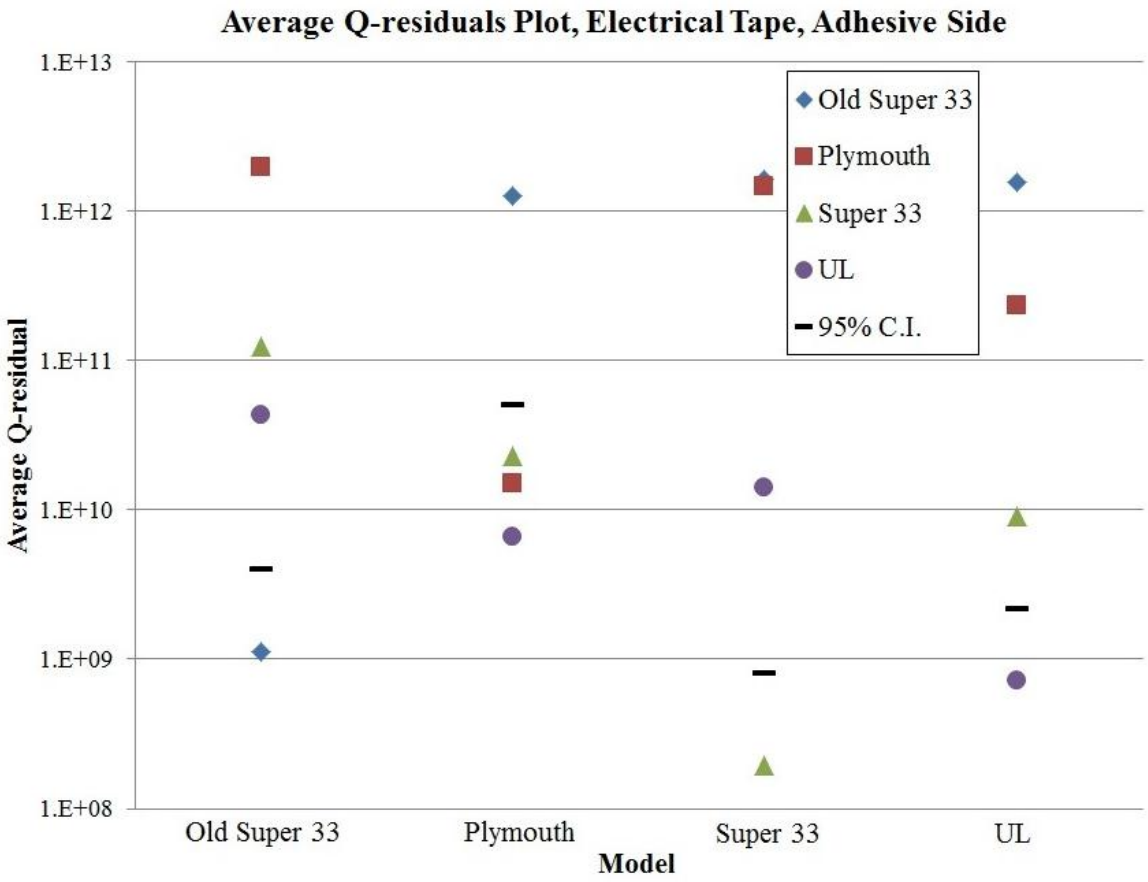


**Figure 16** Average Q-residuals plot for the adhesive side of electrical tape. The black line denotes the 95% confidence interval for each model.

## REFERENCES


1. Bradley, M. J.; Keagy, R. L.; Lowe, P. C.; Rickenbach, M. P.; Wright, D. M.; LeBeau, M. A. A Validation Study for Duct Tape End Matches. *J. Forensic Sci.* **2006,** *51,* 504-508.

2. Keto, R. O. Forensic Characterization of Black Polyvinyl Chloride Electrical Tape. *Crime Lab Digest* **1984,** *11,* 71-74.

3. Kee, T. G. The Characterization of PVC Adhesive Tape. *Proceedings of the International Symposium on the Analysis and Identification of Polymers*, Quantico, VA; Washington D.C., 1984.

4. Mehltretter, A. H.; Bradley, M. J.; Wright, D. M. Analysis and Discrimination of Electrical Tapes Part II: Backings. *J. Forensic Sci.* **2011,** *56,* 1493-1504.

5. Hida, M.; Satoh, H.; Mitsui, T. Comparitive Study of A Cluster Analysis and A Principal-Component Analysis Using a Polarized Imaging Technique for Discriminating Adhesive Cloth Tapes. *Anal. Sci.* **2002,** *18,* 717-722.

6. Goodpaster, J. V.; Sturdevant, A. B.; Andrews, K. L.; Brun-Konti, L. Identification and Comparison of Electrical Tapes Using Instrumental and Statistical Techniques I: Microscopic Surface Texture and Elemental Composition. *J. Forensic Sci.* **2007,** *52,* 610-629.

7. Goodpaster, J. V.; Sturdevant, A. B.; Andrews, K. L.; Briley, E. M.; Brun-Konti, L. Identification and Comparison of Electrical Tapes Using Instrumental and Statistical Techniques II: Organic Composition of the Tape Backing and Adhesive. *J. Forensic Sci.* **2009,** *54,* 328-338.

8. Gray, A. L. Solid Sample Introduction by Laser Ablation for Inductively Coupled Plasma Source Mass Spectrometry. *Analyst* **1985,** *110,* 551-556.

9. Watling, R. J.; Herbert, H. K.; Delev, D. Gold Fingerprinting by Laser Ablation Indictively Coupled Plasma Mass Spectrometry. *Spectrochimica Acta Part B: Atomic Spectroscopy* **1994,** *49,* 205-219.

10. Bajic, S. J.; Aeschliman, D. B.; Saetveit, N. J.; Baldwin, D. P.; Houk, R. S. Analysis of Glass Fragments by Laser Ablation-Inductively Coupled Plasma-Mass Spectrometry and Principal Component Analysis. *J. Forensic Sci.* **2005,** *50,* 1123-1127.

11. Weis, P.; Deucking, M.; Watzke, P.; Menges, S.; Becker, S. Establishing a Match Criterion in Forensic Comparison Analysis of Float Glass Using Laser Ablation-Inductively Coupled Plasma-Mass Spectrometry. *J. Anal. Atom. Spec.* **2011,** *26,* 1273-1284.

12. May, C. D.; Watling, R. J. A Comparison of the Use of Refractive Index (RI) and Laser Ablation-Inductively Coupled Plasma-Mass Spectrometry (LA-ICP-MS) for the Provenance Establishment of Glass Bottles. *Forensic Sci. Med. and Path.* **2009,** *5,* 66-76.

13. Guillong, M.; Gunther, D. Quasi "Non-destructive" Laser Ablation-Inductively Coupled Plasma-Mass Spectrometry Fingerprinting of Sapphires. *Spectrochimica Acta Part B: Atomic Spectroscopy* **2001,** *56B,* 1219-1231.

14. Scheid, N.; Becker, S.; Duecking, M.; Hampel, G.; Volker Kratz, J.; Watzke, P.; Weis, P.; Zauner, S. Forensic Investigation of Brick Stones Using Instrumental Neutron Activation Analysis (INAA), Laser Ablation-Inductively Coupled Plasma-Mass Spectrometry (LA-ICP-MS), and X-ray Fluorescence Analysis (XRF). *Appl. Rad. and Iso.* **2009,** *67,* 2128-2132.

15. Bebe, K. R.; Pell, R. J.; Seasholtz, M. B. Chemometrics: A Practical Guide. John Wiley & Sons: New York, 1998; pp 81-112.

16. Aeshliman, D. B.; Bajic, S. J.; Baldwin, D. P.; Houk, R. S. Multivariate Pattern Matching of Trace Elements in Solids by Laser Ablation-Inductively Coupled Plasma-Mass Spectrometry: Source Attribution and Preliminary Diagnosis of Fractionation. *Anal. Chem.* **2004,** *76,* 3119-3125.

17. SWGMAT. Guidline for Forensic Examination of Pressure Sensitive Tapes. http://www.swgmat.org/Pressure%20Sensitive%20Tape%20guideline.pdf (accessed February 2012).

18. Braeunling, E. *Handbook of Pressure Sensitive Tapes,* 3rd ed.; Van Norstrand Reinhold: New York, 1999; pp 643-660.

19. Houk, R. S.; Fassel, V. A.; Flesch, G. D.; Svec, H. J.; Gray, A. L.; Taylor, C. E. Inductively Coupled Argon Plasma as an Ion Source for Mass Spectrometric Determination of Trace Elements. *Anal. Chem.* **1980,** *52,* 2283-2289.

20. Jolliffe, I. T. *Principal Component Analysis,* 2nd ed.; Springer: New York, 2002.

21. Shlens, J. A Tutorial on Principal Component Analysis Derivation, Discussion and Singular Value Decomposition, 2003. http://www.cs.princeton.edu/picasso/mats/PCA-Tutorial-Intuition_jp.pdf (accessed November 2, 2012).

22. Gunther, D.; Koch, J. Femtosecond Laser Ablation Inductively Coupled Plasma Mass Spectrometry: Achievements and Remaining Problems. *Anal. Bioanal. Chem.* **2007,** *387,* 149-153.

# Chapter 4. Elemental Analysis of Pigments Found in the Shipwreck of *La Belle*

A chapter from the book entitled: *La Belle: The Archaeology of a 17th Century Ship of New World Colonization*

*Megan L. Mekoli[1], Eric D. Ray[2], and Cameron R. Sheya[3]*

*[1]Iowa State University, Ames, Iowa 50011*
*[2]Corpus Christi Museum of Science and History, Corpus Christi, Texas 78401*
*[3]Vienna, Austria 1220*

## INTRODUCTION

During excavation, a variety of pigments (Table 1) collectively weighing approximately 8 kg, was recovered from *La Belle*'s hull. The pigments were located amidships in the main hold and in the aft hold. While the majority may represent the contents of Box 9 (Artifact No. 5110), others were found in a variety of contexts, including Cask 10, and a very small amount contained in a bark bag in the ship's aft hold (Artifact No. 10312, Pigment E).

The pigments vary in color and texture, including a brilliant red, a rust red, and a sandy yellow. They were collected during fieldwork and later transferred to storage at the Corpus Christi Museum of Science and History for curation and future analysis. Elemental analysis determined a majority of the pigments contain different amounts of vermilion (HgS/cinnabar), which was used extensively by the French and other explorers in North America as a trade item. Except for one pigment (pigment F), all the vermilion samples were adulterated with iron or red lead, a very common practice at the time. Other pigments present are likely ochre ($Fe_2O_3$). Two samples were not analyzed for this study but are similar in appearance to the vermilion-containing pigments.

***Use and Composition of Vermilion***

Vermilion has been used as a pigment since antiquity. It is referred to several times in the Bible (New American Standard Bible, Jer. 22:14, Ezek. 23:14) as a paint pigment, alluded to in the *Odyssey* as a pigment for ship paint, [1] and scientifically documented on two Ptolemaic-era Egyptian masks. [2] While not known to be on shipwreck sites other than *La Belle*, in the context of New World exploration it was commonly carried by explorers and colonists as a trade or gift item.

In 1701, the d'Iberville expedition took 80 *livres* (roughly 39 kg) of vermilion to Louisiana, [3] and vermilion was a common gift item on that expedition. In 1765 along the Great Lakes, one pound of vermilion was worth two beaver pelts, roughly the same as eight quarts of rum. [4] Vermilion remained a staple of exploratory trade into the nineteenth century, when Lewis and Clark brought two pounds. [5]

On the La Salle expedition, vermilion was used as both a gift and trade item, carried in lots consisting of "hatchets, knives, awls, glass beads, vermilion, and several other things...". [6] Vermilion is an intense red, much brighter than the rust-colored ochre available in the New World. Thus, this would have been an attractive luxury item for native New World residents.

As a naturally occurring mineral pigment, vermilion is known as cinnabar (HgS) and is found within mineral assemblages in epithermal systems throughout the world. Epithermal mineralization occurs in relatively low temperatures, ranging from 50-300$^{o}$C [7, 8] and in environments close to the surface, usually within the first 800 meters (Figure 1). [7, 9] This particular environment of formation is also preferred by a suite of other minerals including pyrite (FeS), marcasite (FeS), sphalerite ((Zn,Fe)S), galena (PbS), chalcopyrite ($CuFeS_2$),

jamesonite ($FeSb_6S_{14}$), stibnite ($Sb_2S_3$), realgar ($As_4S_4$), orpiment ($As_2S_3$), and argentite ($Ag_2S$). [9] Epithermal systems, are known for their concentrations of elements and heavy metals such as Pb, Zn, Hg, Ag, Au, Sb, Cu, Se, Bi, U, and Sb (Figure 1). [9, 10, 11]

Epithermal systems are almost always associated with volcanism or plutonism, as the original sulphic aqueous brine is derived from magmatic sources, and solutes are gained from the magma, gases from the magma, and the host rock itself. [7, 12] The sulfur in the system is derived from the intrusive body releasing $SO_2$ which then travels either with the magmatic brines from the intrusive body itself, is mixed with deeper aquifers that interact directly with the plutonic body, or from meteoric waters near the surface (Figure 1).

As the brine travels from the source of magma emplacement, it requires a transport system to bring the brine and dissoved minerals to the surface. This is usually accomplished by fault planes or fracture networks. The fluids are pushed towards the surface by the convection of the magma emplacement and the relative buoyancy.The cooling of the fluids results in the precipitation of certain minerals at particular temperature regime. [7, 9] The different precipitation temperatures and relative concentrations of compounds within the brine dictate what mineral assemblages are present at particular pressure, depth, and temperature regimes.

The formation of cinnabar is also closely linked to hotsprings, indicating that a $B_2$ type mixing of meteoric waters is the most common mode of formation. This also indicates that the associated minerals will be most commonly marcasite and stibnite [13] and should be expected in any natural sample containing cinnabar. Because cinnabar and other epithermal minerals are formed close to the surface, mining is less costly, and in cases such as in underwater plutonism and volcanism, hotsprings, and geysers, mineralization is possible

within the first 100 meters of rock at high temperature hydrothermal alteration zones such as in the Western Pacific floor. [14]

The two most economically-valuable zones in a hydrothermal system are where the base and precious metals are precipitated, usually in the higher temperature regime of the mesothermal system. This results in mainly Au, Ag, and Cu being precipitated in areas such as the brecciated zones where fault planes converge (Figure 1). [9] This mode of precipitation is what forms the main gold-bearing veins found in the Sierra Nevada mountains in California, and the vein gold deposits found throughout Alaska.

Depending on the country rock and type of magma (felsic, mafic), different mineral assemblages will be present in differing concentrations and percentages. However, there are always certain accessory ores and minerals that are associated with cinnabar, as is seen in Figure 1.

Because of the process of aqueous circulation, origin of brines, and deposition circumstances, it is exceedingly difficult to get any large quantity of any certain material in pure form with no inclusions or adulturations from the surrounding host rock. Again, any naturally occurring cinnabar should have the other aforementioned associated minerals occuring alongside.

Mined cinnabar can be ground into powder and used directly as a dye (in which case it is "natural" vermilion). However, the many accessory minerals invariably contained in natural vermilion create an impure pigment, and so a method for creating synthetic vermilion was created which produces a pigment free from these natural impurities. A Dutch manuscript from the seventeenth century describes the "Dutch process" of making synthetic vermilion. The process, described in great detail, involves cooking pure mercury (derived

from natural cinnabar) and pure sulfur.[15] As injurious to health as this process must have been, it created vermilion free from any impurities, containing only mercury and sulfur.

Due to the expense of the synthetic method, vermilion produced in that fashion was frequently adulterated with brick dust, ochre, or red lead. The 15th century painter Cennini advises: "always buy vermilion unbroken, and never pounded or ground. The reason? Because it is generally adulterated, either with red lead or with pounded brick." [16] In 1758, Robert Dossie [17] (45) writes that it is "very usual, dare I say general, for dealers to sophisticate vermilion with red lead," and details methods for detecting this fraud. Likewise, in 1773 lead is implicated as an adulterant, affecting vermilion's drying properties. [18] The more adulterated pigments would cost less, as they required less of the expensive pure mercury.

**RESULTS AND ANALYSIS**

As a means to determine if the pigments from *La Belle* were vermilion, and to discover their purity, elemental analysis was conducted to determine the elemental makeup of the material. As the fraudulent pigment salesmen cited in primary literature knew, other similarly colored substances, such as magnetite ($Fe_2O_3$, iron (III) oxide, red ochre) or red lead ($Pb_3O_4$, lead tetroxide) can easily be mistaken for vermilion. Pigment samples found on *La Belle* were analyzed using inductively coupled plasma-mass spectrometry (ICP-MS). The instrument was first described by Houk *et al.* [19] at Iowa State University and has uses in environmental studies of water quality, trace analysis in forensic science, purity determination of silicon wafers used in technology manufacturing, and many other areas.

Twelve pigment samples were analyzed using ICP-MS; sample proveniences are illustrated in Figure 2. Samples still wet with seawater were air dried so that water would slowly evaporate from the solid.

ICP-MS is a sensitive chemical analysis technique wherein a plasma (i.e., a high temperature electrical discharge) acts as a source of sample ionization. ICP-MS was chosen to analyze the samples over other elemental analysis techniques due to its low limits of detection (LOD). It is common to analyze samples with an analyte (the substance being measured) concentration in the low ppb (parts-per-billion) range. For some elements in certain conditions, LOD as low as ~1 ppt (part-per-trillion) can be achieved. ICP-MS also provides isotopic data on the elements present in the sample whereas competing elemental instrumentation usually only provides information on the particular element present. However, ICP-MS does not provide information on the chemical form of the elements present. Instead of detecting HgS (vermilion), ICP-MS can only detect the presence of Hg or S. ICP-MS is capable of measuring multiple isotopes rapidly. A caveat to solution-based ICP-MS, the kind of analysis performed here, is that it does not provide spatial information within a single analyzed sample because the entire sample is evenly mixed into the solution.

The plasma breaks up a sample into singly-charged atomic ions using numerous collisions. To create this plasma, a high voltage radiofrequency current is passed through a coil, which induces an alternating magnetic field on the inside of the coil. A spark creates initial ions from an inert gas (usually Ar, N, or He) that flows through a diffused quartz torch at the center of the coil. The alternating magnetic field influences the motion of free electrons on the inside of the coil such that the electrons collide with gas atoms, creating intense heat and more ions. The resultant gaseous atoms, ions, molecules, and electrons is called a

plasma. The temperature of the plasma is approximately 7,000 K, roughly the temperature of the surface of the sun, and can vary due to factors such as the elements being measured, the number of collisions generated, and other instrumental conditions. The sample and the inert sample gas are atomized (broken up) and ionized in the plasma.

From the plasma, the atomized sample ions are passed into a high resolution ELEMENT 1 ICP-MS device (Thermo Inc.) (Figure 3) where they are separated by momentum (mass*velocity) using a curved flight tube between two magnet pole pieces called a magnetic sector analyzer (Houk 2003). The ions are then processed by the electrostatic analyzer (ESA) where they are further separated and refocused onto the detector based on their respective kinetic energies (0.5mass*velocity$^2$). The particular arrangement of the magnetic sector followed by the ESA in the instrument used is called a "reverse Nier-Johnson" configuration. Using both separation techniques, the resolution is high enough to separate chemically different ions at the same nominal mass, such as $^{56}Fe^+$ from $^{40}Ar^{16}O^+$. After they pass through the ESA, the ions hit an electron multiplier where the signals are amplified and detected. In mass spectrometry, detected ions can have multiple charges and data are analyzed based on the mass-to-charge ratio, however, ICP-MS mainly produces single positively charged ions due to the conditions in the plasma. Intensities for a given mass typically correlate to the isotope mass for the measured element. Polyatomic ions, such as $^{40}Ar^{16}O^+$ occur often and can interfere with isotopes of desired atomic ions (such as $^{56}Fe$), however, this instrument has the capacity to resolve many of these interferences.

A 50-mg sample of each pigment was dissolved in cleaned, concentrated aqua regia a 1:3 (v:v) mixture of clean nitric acid [$HNO_3$] and hydrochloric acid [HCl], (Ultrex II, ultrapure reagents). The percentage of the entire sample varied. In some cases, 50 mg

represents a significant portion of the artifact. In most cases, 50 mg represents only a tiny fraction of the hundreds of grams present in the collected sample. Once the pigments were dissolved, they were diluted to roughly 10 ppm (parts-per-million) and then to approximately 10 ppb (parts-per-billion) in an aqueous solution of approximately 2% aqua regia. Pigments were dissolved and diluted using nanopure water (18 MΩ, Millipore) in cleaned Teflon bottles (which were cleaned via acid vapor washing. Care was taken during the dissolution process to retain as much mercury from the samples as possible. Mercury is volatile and at high temperatures can be easily lost from open vessels at high temperatures. Pigments were thus allowed to slowly dissolve over a period of 12 hours in tightly-sealed containers.

Samples were analyzed using a Thermo ELEMENT 1 ICP-MS device. Instrument parameters are listed in Table 3. In many cases, multiple isotopes were measured for each element to confirm the presence of the element, as opposed to a polyatomic interference ion, and to check the agreement of the final calculations. Initially, a full spectrum scan in medium resolution ($m/\Delta m=4000$) was conducted on both the 10 ppm and 10 ppb sets of dissolved vermilion to screen for the elements present. It was determined that the 10 ppb solution was too dilute to detect the presence of non-bulk, or trace, elements so the 10 ppm solution was used for quantification.

Raw data were peak integrated, averaged and background subtracted. Elements detected in the 10 ppm solutions were quantified by comparing 50 intensity measurements of diluted sample isotopes to those of a standard solution with the same solvent composition. Arsenic (As) and sulfur (S) were measured using high resolution ($m/\Delta m=10000$) due to overlapping interference peaks at masses 32 and 75. A list of elements analyzed for quantification is below.

The measured signals were converted into weight percent in the original solid sample. A list of the measured concentrations for each element in the pigments can be found in Table 2. Standard deviation values (in percent) of 10 consecutive measurements of the analysis are also shown. The standard deviations were low for bulk components (such as Hg, Fe and Pb) in the pigments. For trace components under 1% of the sample, the standard deviation values are larger due to the instability of the signal at lower count rates.

**DISCUSSION**

A plot chart illustrates the measured concentrations of all elements found in abundance greater than 1% by weight in any of the pigments (Figure 4). Error bars indicate the standard deviation (in percent) of 10 consecutive measurements of each isotope; many of the error bars are smaller than the plotted points. Table 2 indicates that many elements were initially found in the pigments, however the scope of this study was to measure larger bulk components (defined here to be 1% (w/w) or greater of the pigment) and not trace or ultra-trace components. These results shed light on the composition of each pigment, which in turn gives information about the artifacts' origins.

From the ICP-MS results, it was apparent that none of the more obvious precious metals expected to accompany natural cinnabar were present in the pigments, even in small amounts. Attention was then turned to arsenic, a constituent of extremely common accessory minerals. Pigment samples were analyzed using high resolution ($\Delta m/m=10000$) to resolve $^{75}As^{+}$ from an interference peak of $^{40}Ar^{35}Cl^{+}$. No As was detected at a level above the blank in any of the pigments when As was measured using high resolution (results not shown). This does not however indicate that As was absent in the pigments. Roughly 80% of the medium

resolution signal is lost when switching from medium resolution to high resolution on the ELEMENT 1, making the limit of detection (LOD) for high resolution roughly 80% higher than that of medium resolution. If As is in the sample, it will be in quantities lower than the LOD for high resolution. Another caveat of trying to detect As is that As only has a 52% ionization efficiency. [20] This means that only 52% of the total As is ionized and eligible for detection in the instrument. However, even if only half the As was detected, it still would not represent even close to the amount expected in natural cinnabar. Thus, in the absence of any accessory elements, the vermilion on *La Belle* must be synthetic rather than natural.

If the pigments were all truly pure vermilion, they would all contain both Hg and S, to the exclusion of other elements. However, this is not the case. A sample of pure vermilion has a stoichiometric Hg:S ratio of 1:1. Table 4 is the molar ratio of Hg/S calculated for all pigments, with the exception of pigment C, which was discarded before S content could be measured. Ideally, the molar ratio value would be exactly 1; however, this was not observed. Most pigments with the largest component being Hg or Pb had a molar ratio (Hg/S) value that was less than 1. Molar ratio values that were less than 1 indicate there was less Hg or more S than expected; possibly owing to poor Hg recovery during dissolution, additional S contamination that was not originally from the pigment, such as biogenic S, or a combination of both.

It is well-documented that maritime artifacts often contain large amounts of biogenic S, [21, 22, 23] Bacteria found on the seafloor can reduce sulfate ions found in organic matter to hydrogen sulfide, $H_2S$. Dissolved $H_2S$ can readily react with reduced S compounds in the wood and other artifacts, (such as HgS), and become incorporated into the material itself. This process can depend on the concentration of $H_2S$ available, how readily the wood is

degraded, or the amount of corroding iron, which can serve as a reducing agent of S compounds. [21, 24]

Molar ratio values greater than 1 (as is the case of pigment F) indicate there was more Hg present than expected, less S than expected, or both. All pigments but one contained some amount of Hg and S, while L did not contain any Hg at all.

When all percentages of contributing elements are added together, the resultant value does not equal 100% (except for in the case of pigment F). This discrepancy is due to the large amount of organic material that was not analyzed. It is difficult to track whether organic material came from the pigments themselves or from the ocean, where the pigments sat for so long. Silicon (Si) is a main component of sand ($SiO_2$) and was also not measured in these samples. $SiO_2$ sediments adding contamination to the pigments from the ocean floor is also likely.

Figure 5 is a plot of the four largest components in each pigment analyzed. Samples L and E in Figure 5 contain little- to no Hg, but have a very high percentage of Fe. These two pigments were likely magnetite, also known as ochre ($Fe_2O_3$), which is difficult to distinguish from vermilion without modern analysis techniques.

Lead (Pb), an adulterant so common as to be general in the seventeenth century, was found in many of the samples analyzed. Most pigments which contained measureable amounts of Hg also included measureable amounts of Pb, but usually in a lower quantity than Hg. Figure 5 and Table 2 indicate the amounts of Pb present in the pigments. Sample K actually contained higher amounts of Pb (30.1%) than Hg (28.0%). Pigments L and E did not contain Hg but did contain a very high content of Fe (55.3% and 38.7%, respectively). Pigment L is the yellow pigment, and its high Fe content shows that this is yellow ochre

(hydrated iron oxide). These two samples did not contain large quantities of Pb, indicating they were not adulterated with Pb. While Pb is a common contaminant in elemental analyses, these high concentrations are not indicative of contamination, but of adulteration present in the pigments themselves. This matches with the historical accounts indicating that red lead was ubiquitous as an adulterant.

In pigment F, there are only very low levels of impurities (such as Mg and Fe) and no significant levels of accessory elements. The total percent composition of Hg and S in pigment F is 101%. When the impurities are added to the amounts of Hg and S, the total percent composition of F is 107%. While this very pure pigment should read 100%, the measured value of 107% is within precision of the values of all the elements measured. The levels of impurities are low enough to be considered trace, indicating that pigment F is high purity vermilion (HgS). The lack of impurities suggests the vermilion was produced using the Dutch process. Thus, *La Belle's* pigments provide direct evidence for a synthetic origin of at least some of the vermilion accompanying French colonial efforts.

Pigment H did not contain appreciable levels of the elements measured (Fe, Pb, or Hg). This particular sample likely contained a higher percentage of organic material (C, N, O, etc.) that is removed by acid digestion and thus difficult to determine using ICP-MS. Pigment H likely contained a large amount of Si mixed in from the sand on the floor of the bay, where the samples had been sitting for over 300 years.

The sample taken from the bark bag in the aft hold (pigment E) is primarily Fe. It also contained a rather large abundance of chromium (Cr) at 8.52% and nickel (Ni) at 4.18% by weight in the original solid. Pigment K similarly contained higher abundances of Cr and Ni than many of the other pigments with 3.56% and 1.82%, respectively. However, K

contained Hg at 28.0% whereas the Hg concentration of E was less than 1.5% of the original mass. The origin of the high levels of chromium and nickel is not known, and requires further research.

Tantalizingly, both nickel and chromium are found as natural contaminants in parts of Quebec, [24] suggesting a possible association with native ochre from La Salle's previous journeys to Canada – perhaps the birch bag contains European vermilion mixed with North American ochre. For the moment, this is nothing more than a suggestive possibility, and will require further research.

**CONCLUSIONS**

The chemical and geological analysis of *La Belle's* pigments provides information to better understand the larger story of the La Salle expedition. Of the twelve pigments analyzed, nine (pigments A,B,C,D,F,G,H,I,J) have as their primary coloring agent mercury, as opposed to red lead or iron oxide. Two (pigments E and L) are primarily iron oxide, and one (pigment K), is primarily red lead.

The spatial arrangement of the pigments (Figure 2) reveals that the analyzed pigments were primarily clustered together, and mostly found in the vicinity of Box 9. Those directly associated with Box 9 are A,C,K,D,I,G. While pigments H and J were not directly identified as components of Box 9, they are close enough that they may originally have been part of this box's contents. Pigment F is nearby, but was found associated with Cask 10, a cask primarily containing tools and dry goods.

Of the three outlying pigments, one (pigment L) is the sample of yellow pigment, and is primarily colored with iron. The other iron-dominant pigment (pigment E) is also an outlier. This is the sample of ochre from in the birch bag, and was in the aft hold, near the crew's presumed living and recreation area. The final outlier (pigment B) is a mercury-dominant pigment, and was in the stern portion of the ship, possibly originally in the stern cabin.

Comparing the chemical compositions across different provenience areas presents an intriguing line of inquiry. The large amount of pigment present in and around Box 9 suggests that this was the expedition's primary supply. If the La Salle expedition had intended their pigment supply to be homogenous in quality, the chemical composition would be consistent throughout, which would be indicative of a well-mixed powder. Instead, the pigments in this box have varying amounts of mercury, iron, and lead. Certainly the pigment present in this box is not high-grade vermilion. All the samples had significant amounts of adulterant (lead and iron) compared to their mercury percentage. In fact, pigment K is primarily red lead (30% Pb vs 28% Hg). The heterogeneous nature of the pigments in Box 9 shows that there were different grades present in the box, ranging from the relatively high-quality (pigment A, 60% Hg vs. 5.5% Pb) to the extremely low-quality (the aforementioned primarily-lead pigment K).

The very pure vermilion (pigment F) was in Cask 10, rather than in the trade box. This suggests that someone on the expedition was cognizant of the difference in quality, and made an attempt to keep this expensive good separate. While it is impossible to know for sure, pigment F may not have been meant for trade, but rather for domestic use. Outside of the trade box and cask 10 pigments, the yellow ochre was kept separately, but still in the

main hold. Perhaps this was a personal supply, or simply a different trade item. The tiny amount of ochre present in the birch bag, along with its location in the aft hold, suggest that this was not part of a large trade supply, but was a personal item or keepsake. Finally, pigment B, tentatively associated with the stern cabin, may represent part of the ship's ready "currency", easily accessible in case of immediate need.

The absence of the usual accessory elements (such as gold or arsenic) in any of the pigments proves that the vermilion used was synthetic, rather than naturally occurring cinnabar. Unfortunately, this also means no geographic origin can be suggested, as would be possible with natural cinnabar. However, it is indicative of a manufacturing process that takes natural ore, refines it to pure mercury, recombines that mercury with sulfur to produce synthetic vermilion, and then (in all but one case), adulterates the resulting product with cheaper lead or iron, suggesting that this trade item underwent a large amount of processing before arriving on New World shores.

## TABLES

**Table 1** Pigments analyzed by inductively coupled plasma-mass spectrometry

**Pigments Analyzed**

| Sample ID | Pigment Letter | Easting | Northing |
|---|---|---|---|
| 3335 | A | 2010 | 2016 |
| 3385-4 | B | 2009 | 2010 |
| 7025 | C | 2010 | 2016 |
| 7951 | D | 2010 | 2016 |
| 10312 | E | 2009 | 2013 |
| 10490 | F | 2009 | 2016 |
| 10548 | G | 2010 | 2016 |
| 10555 | H | 2010 | 2017 |
| 10747 | I | 2010 | 2016 |
| 10973 | J | 2010 | 2017 |
| 11086 | K | 2010 | 2016 |
| 11799 | L | 2011 | 2015 |

**Table 2** Instrumental parameters for the quantitative ICP-MS measurements

**Instrumental Parameters for the Quantitative ICP-MS Measurements.**

| | |
|---|---|
| ICP-MS model | ELEMENT 1 (Thermo, inc.) |
| Sampler and skimmer cones | Ni, H configuration (Thermo, inc.) |
| Nebulizer | 100 µL $min^{-1}$ (Elemental Scientific, inc.) |
| Sample gas | 1.077 L Ar $min^{-1}$ |
| RF Power | 1150 W |
| Cool/auxiliary gas stream | 16.00/1.16 L Ar $min^{-1}$ |
| Torch position, ion optics | Optimized for maximum sensitivity and stability |
| Scan mode<br>dwell/settling time | Peak jump, 20 points per mass, 10 ms dwell time, 2.1 ms settling time |
| Acquisition (Runs/passes) | 10 runs/1 pass |
| Elements measured (medium resolution, unless otherwise noted) | S*, Mg, Al, Sc, Ti, V, Cr, Mn, Fe, Co, Ni, Cu, Zn, Ga, As*, Rb, Sr, Y, Zr, Mo, Ag, Sn, Sb, Te, Ba, Ce, W, Au, Hg, Tl, Pb, U<br>*Measured in high resolution |

**Table 3** Concentration of Element (%, w/w) in Each Pigment

| | Element Concentration (%) in Each Pigment | | | | | | |
|---|---|---|---|---|---|---|---|
| **Sample** | S | Mg | Cr | Fe | Ni | Hg | Pb |
| **A** | 11.1 ± 0.8* | 0.423 ± 0.017 | 0.248 ± 0.009 | 0.627 ± 0.017 | 0.084 ± 0.005 | 60.3 ± 1.5 | 5.58 ± 0.17 |
| **B** | 1.74 ± 0.18 | 0.419 ± 0.013 | 0.044 ±0.002 | 4.56 ± 0.13 | 0.021 ± 0.002 | 7.67 ± 0.18 | 3.23 ± 0.11 |
| **C** | N/A | 0.057 ± 0.003 | 0.076 ± 0.006 | 0.406 ± 0.016 | 0.028 ± 0.003 | 53.1 ± 1.9 | 35.372 ± 1.348 |
| **D** | 0.0668 ± 0.075 | 0.305 ± 0.010 | 0.005 ± 0.001 | 1.30 ± 0.04 | $0.002 \pm 0.000_4$ | 3.44 ± 0.08 | 0.901 ± 0.024 |
| **E** | 0.661 ± 0.036 | 0.092 ± 0.003 | 8.52 ± 0.26 | 38.7 ± 1.2 | 4.18 ± 0.18 | 1.38 ± 0.04 | 0.286 ± 0.010 |
| **F** | 12.0 ± 5.3 | 2.71 ± 0.16 | 0.441 ± 0.034 | 1.92 ± 0.09 | 0.216 ± 0.021 | 89.3 ± 5.3 | 0.831 ± 0.053 |
| **G** | 2.82 ± 0.22 | 0.382 ± 0.015 | 0.072 ± 0.004 | 2.88 ± 0.08 | 0.026 ± 0.003 | 8.23 ± 0.23 | 3.08 ± 0.11 |
| **H** | 0.234 ± 0.032 | 0.031 ± 0.001 | $0.005 \pm 0.000_2$ | $0.016 \pm 0.000_4$ | $0.004 \pm 0.000_2$ | 1.21 ± 0.03 | 0.923 ±0.025 |
| **I** | 8.55 ± 2.1 | 2.17 ± 0.09 | 0.211 ± 0.009 | 0.749 ± 0.023 | 0.091 ± 0.008 | 49.6 ± 2.1 | 15.7 ± 0.63 |
| **J** | 2.74 ± 0.81 | 0.237 ± 0.015 | 0.314 ± 0.021 | 2.33 ±0.08 | 0.157 ± 0.013 | 16.8 ± 0.8 | 12.5 ± 0.83 |
| **K** | 7.21 ± 0.79 | 0.967 ± 0.039 | 3.56 ± 0.16 | 17.9 ± 0.6 | 1.82 ± 0.07 | 28.0 ± 0.8 | 30.084 ± 0.941 |
| **L** | 0.111 ± 0.014 | 0.076 ± 0.004 | 0.690 ±0.020 | 55.3 ± 1.8 | 0.270 ± 0.017 | < blank | 0.073 ± 0.005 |

* Standard deviation (%, w/w) of 10 consecutive measurements

**Table 4** Molar ratio (Hg/S) values of each original pigment.

**Molar Ratio (Hg/S) Values of Each Original Pigment**

**(The value of pure vermilion, HgS, should be 1)**

| Sample ID | Molar ratio (Hg/S) |
|---|---|
| **A** | 0.863 ± .015 |
| **B** | 0.700 ± 0.002 |
| **C** | N/A |
| **D** | 0.814 ± 0.001 |
| **E** | $0.329 \pm 0.000_2$ |
| **F** | 1.18 ± 0.06 |
| **G** | 0.462 ± 0.002 |
| **H** | $0.819 \pm 0.000_3$ |
| **I** | 0.918 ± 0.020 |
| **J** | 0.970 ± 0.008 |
| **K** | 0.614 ± 0.006 |
| **L** | Not enough Hg |

**FIGURES**

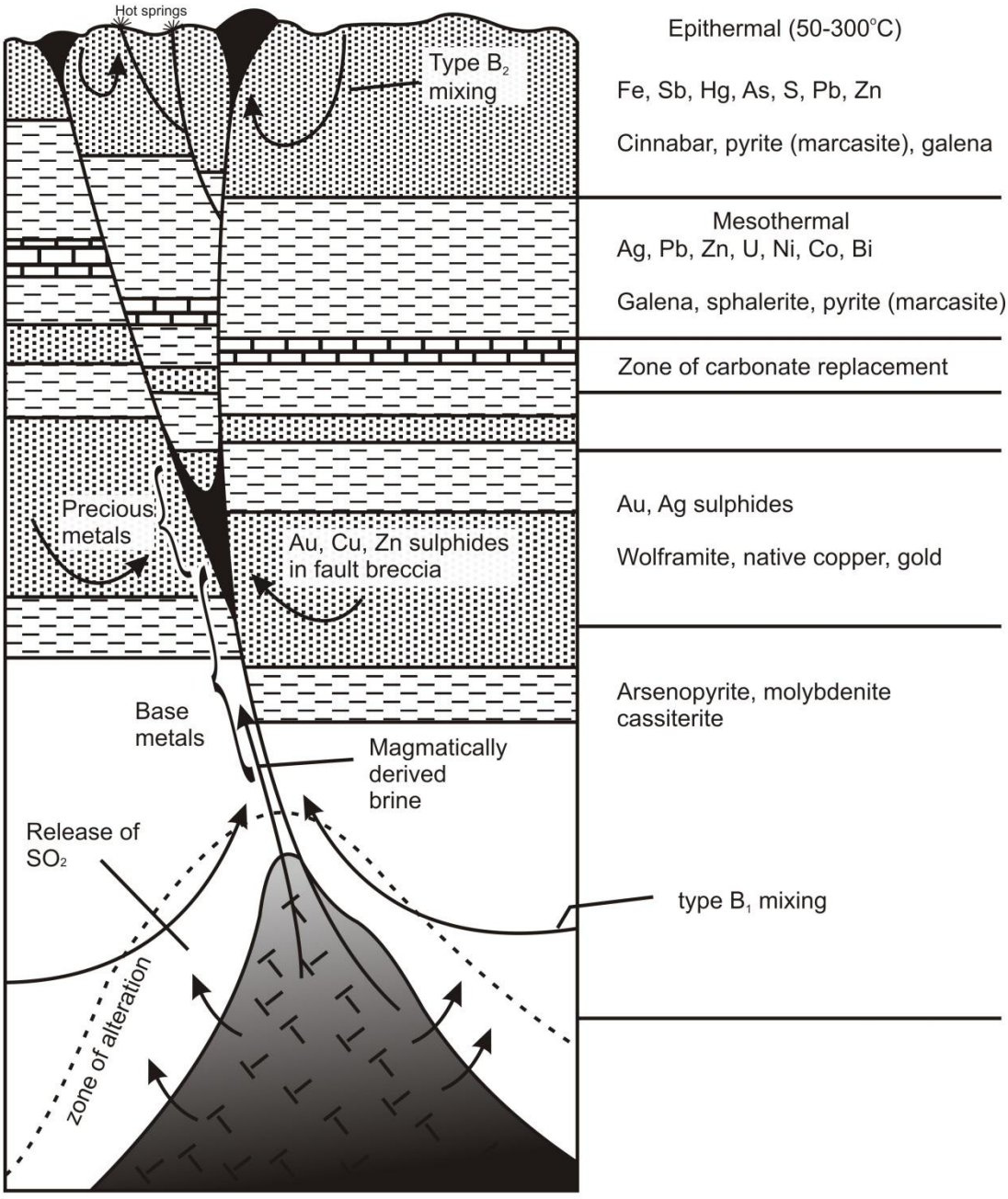


**Figure 1:** Cinnabar formation processes and accessory elements.

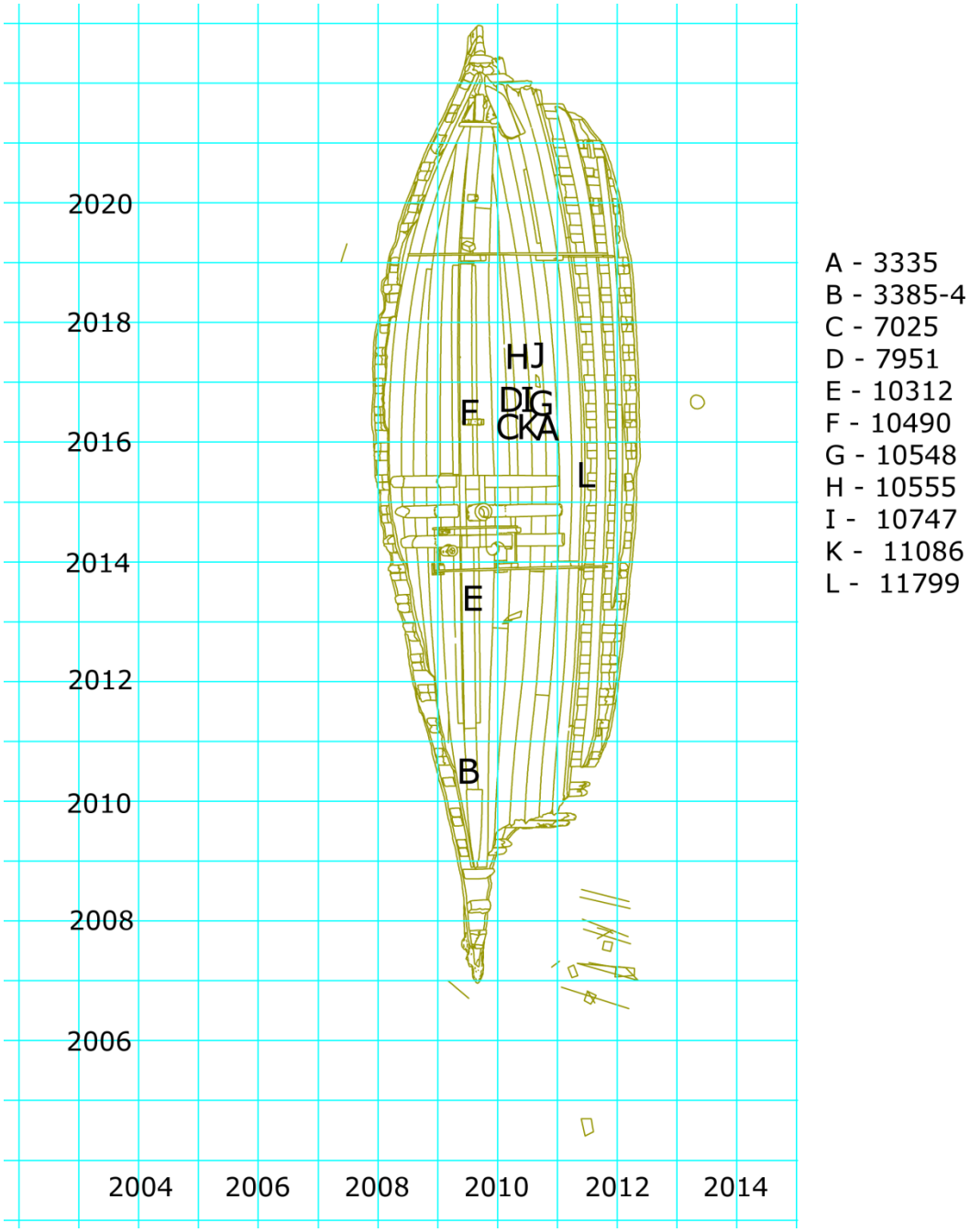


**Figure 2**: Provenience of Pigments.

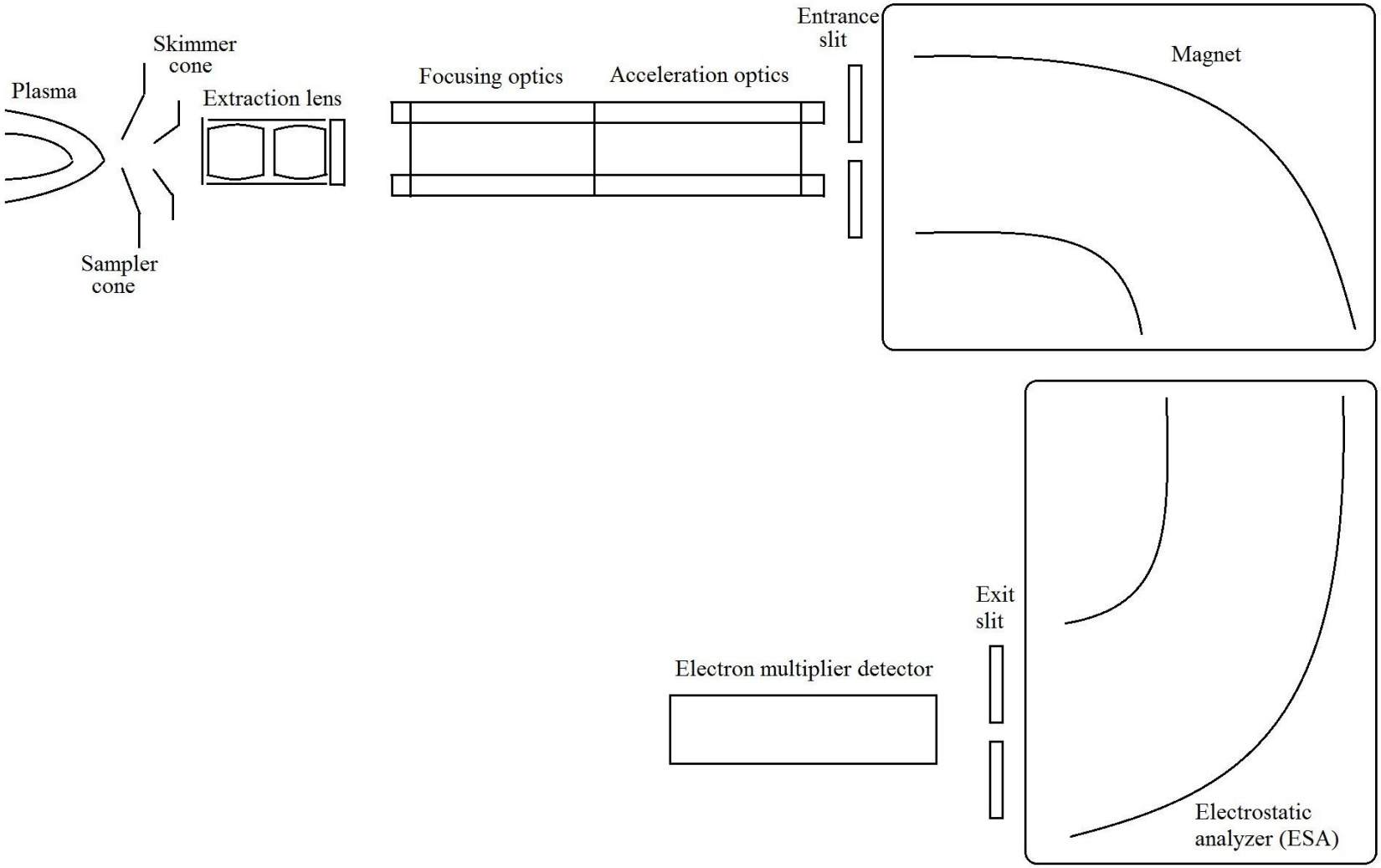


**Figure 3**: Schematic of a reverse Nier-Johnson configuration ICP-MS. Ions are extracted from the plasma through the sampler and skimmer cones by the extraction lens. The beam of ions are focused and accelerated to the magnetic sector analyzer where they are separated based on momentum. These separated ions are further separated based on kinetic energy and refocused to the electron multiplier detector by the electrostatic analyzer (ESA).

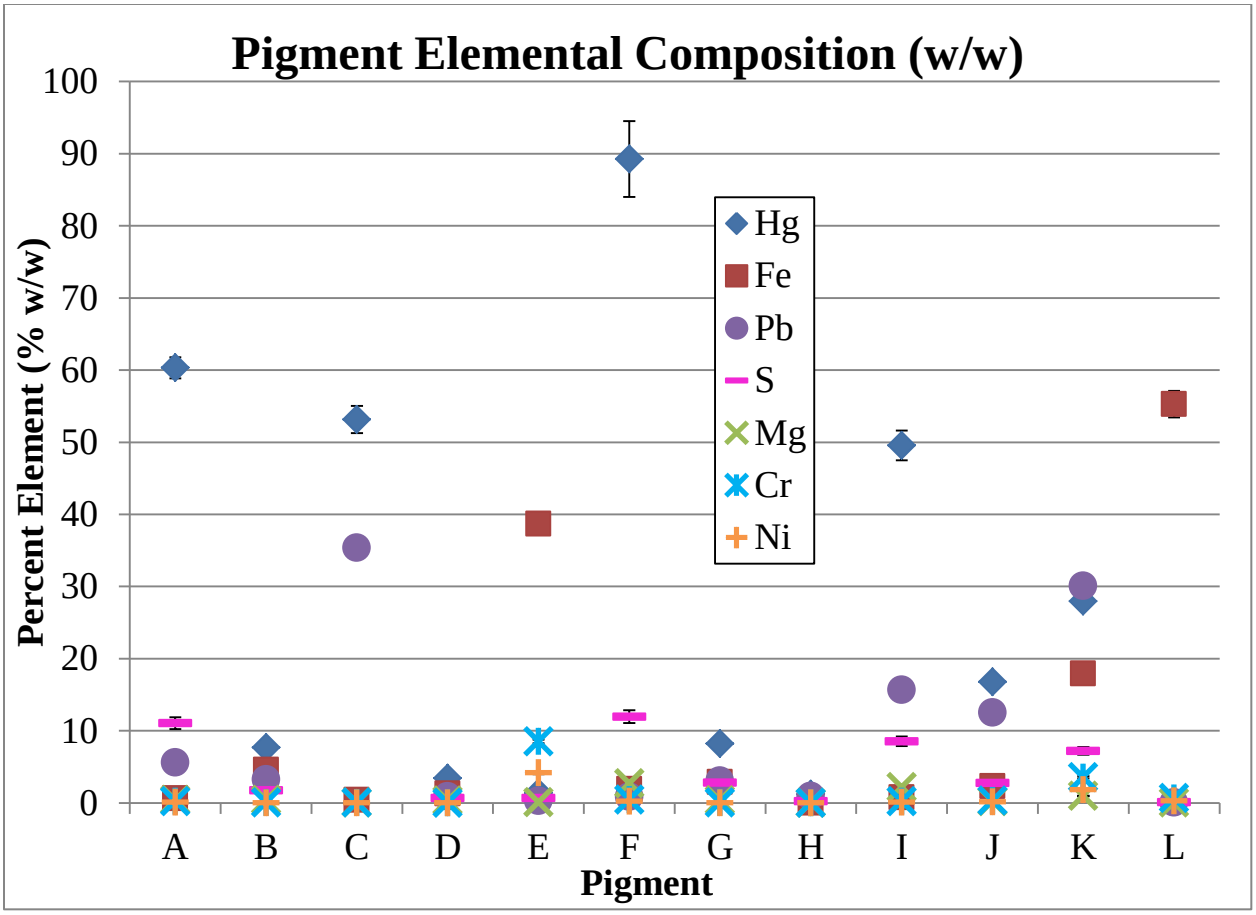


**Figure 4:** Elemental composition of the analyzed pigments. Only elements which contained over 1% by mass (w/w) of any pigment are shown.

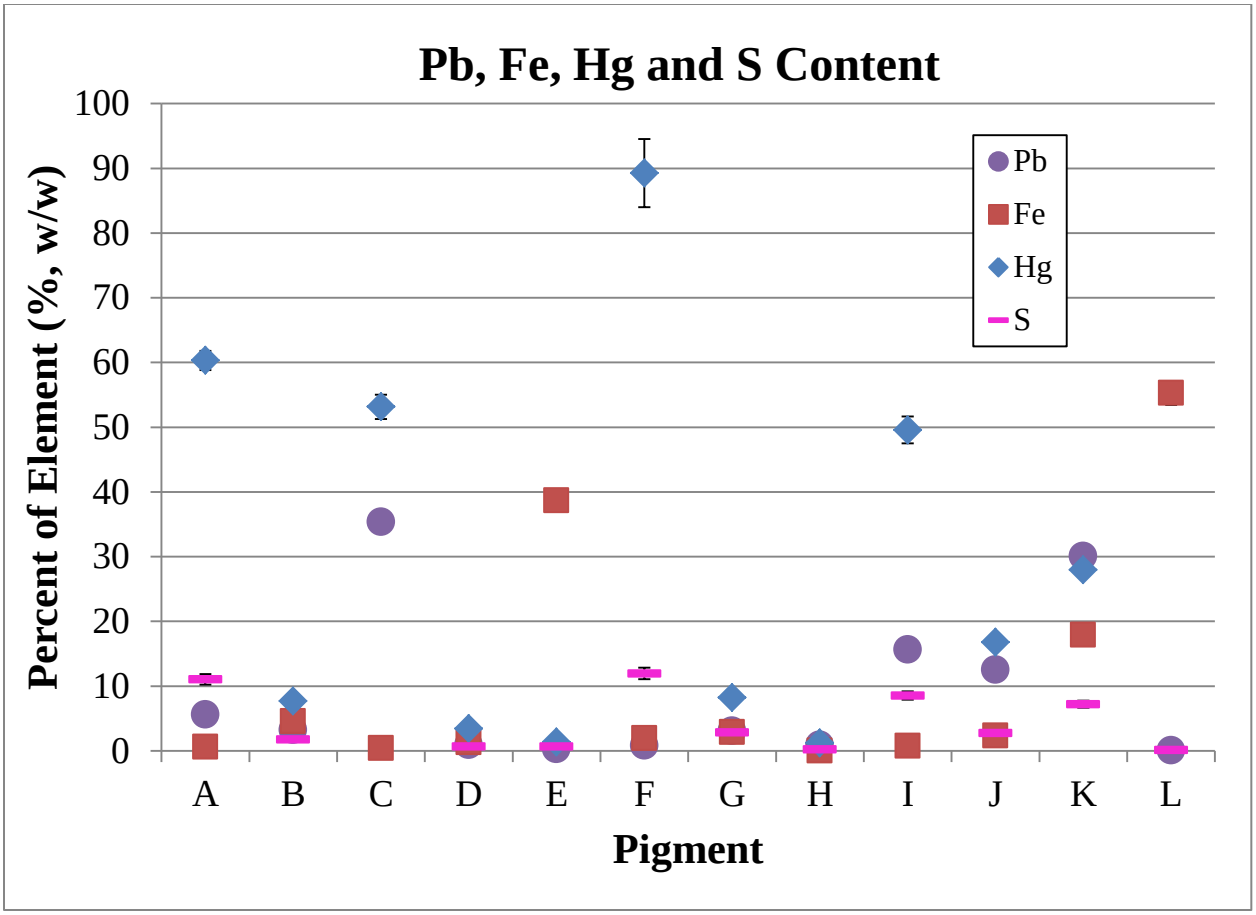


**Figure 5:** Percent (w/w) of mercury (Hg, diamonds), lead (Pb, circles), iron (Fe, squares) and sulfur (S, line) content in 12 pigment samples.

**REFERENCES**


1. Homer. *Homer's Odyssey;* Oxford University Press: Oxford, UK, 1886.

2. Vandenabeeleab, P.; von Vohlenb, A.; Moensa, L.; Klockenkamberb, R.; Joukesc, F.; Dewispelaerec, G. Spectroscopic Examination of Two Egyptian Masks: A Combined Method Approach. *Analyical Letters* **2000,** *33,* 3315-3332.

3. France, L.-D. d. Memoire sur le Mississippi. Le Roi Fair Armer a Rochefort une Frégate et un Batiment de Charge pour le Mississippi. In *Quatrieme Partie: Découverte Par Mar des Bouches Du Mississippi et Etablissements de Lemoyne D'Iberville sur Le Golfe Du Mexique;* Margry, P., Ed.; Maisonneuve et Cio: Paris, 1701; pp 482-486.

4. Purvis, T. L. *Colonial America to 1763;* Facts on File: New York, 1999.

5. Carr, D. *Into the Unknown: The Logistics Preparation of the Lewis and Clark Expedition;* Combat Studies Institute Press: Ft. Leavenworth, KS, 2004.

6. Joutel, H. *The La Salle Expedition to Texas. The Journal of Henri Joutel 1684-1687;* State Historical Association: Austin, Texas, 1998.

7. Arribas, A. Characteristic of High-Sulfidation Epithermal Deposits and Their Relation to Magmatic Fluid. In *Magmas Fluid and Ore Deposits: Mineralogical Association of Canada Short Series,* 23rd ed.; Thompson, J. F. H., Ed.;, 1995; pp 419-454.

8. Hedenquist, J. W.; Arribas, A.; Gonzales-Urien, E. Exploration for Epithermal Gold Deposits: Review. *Economic Geology* **2000,** *13,* 245-277.

9. Evans, A. *Ore Geology and Industrial Minearls: An Introduction;* Wiley Blackwell: Hoboken, NJ, 1993.

10. Berger, B. R.; Henley, R. W. Advances in the Understanding of Epithermal Gold-silver Deposits, With Special Reference to the Western United States. *Economic Geology Monographs* **1989,** *6,* 405-423.

11. Sillitoe, R. H. Gold Deposits in the Wester Pacific Island Arcs: The Magmatic Connection. *Economic Geology Monographs* **1989,** *6,* 274-291.

12. Stoffgren, R. Genesis of Acid-Sulfate Alteration and Au-Cu-Ag Mineralization at Summitville, Colorado. *Economic Geology* **1987,** *82,* 1575-1591.

13. King, R. J. Minearls Explained. *Geology Today* **2002,** *18,* 37.

14. Alt, J. C.; France-Lanord, C.; Floyd, P. A.; Castillo, P.; Galy, A. Low-Temperature Hydrothermal Alteration of Jurassic Ocean Crust, Site 801. *Proceedings of the Ocean Drilling Program*, College Station, TX, 1992; pp 415-427.

15. Van Schendel, A. F. E. Manufacture of Vermilion in 17th-Century Amsterdam. The Pekstok Papers. *Studies in Conservation* **1972,** *17,* 70-82.

16. Cenni, C. D. *The Craftman's Handbook;* Dover Publications: Mineola, NY, 1960.

17. Dossie, R. *The Handmaid to the Arts;* Lamb, London, UK, 1758.

18. Neumann, C.; Lewis, W. *The Chemical Works of Caspar Neumann;* Goldsmith, London, 1773.

19. Houk, R. S.; Fassel, V. A.; Flesch, G. D.; Svec, H. J.; Gray, A. L.; Taylor, C. E. Inductively Coupled Argon Plasma as and Ion Source for Mass Spectrometric Determination of Trace Elements. *Analytical Chemistry* **1980,** *52,* 2283-2289.

20. Niu, H.; Houk, R. S. Fundamental Aspects of Ion Extraction in Induvtively Coupled Plasma Mass Spectrometry. *Spectrochimica Acta Part B* **1996,** *51,* 779-815.

21. Bjordal, C. *Ph.D. Thesis;* Swedish University of Agricultural Sciences: Uppsala, Sweden, 13.

22. Sinninghe Damste, J. S.; de Leeuw, J. W. *Adv. Org. Geochem.* **1990,** *16,* 1077-1101.

23. Sandstrom, M.; Jalilehvand, F.; Damian, E.; Fors, Y.; Gelius, U.; Jones, M.; Salome, M. Sulfur Accumulation in the Timbers of King Henry VIII's Warship Mary Rose: A Pathway in the Sulfur Cycle of Conservation Concern. *Proc. Natl. Acad. Sci. USA* **2005,** *102,* 14165-14170.

24. Klassen, R. A.; Garrett, R. G.; DiLabio, R. Natural Sources of Trace Element Contaminants. In *Threats to Sources of Drinking Water and Aquatic Ecosystem Health in Canada. NWRI Scientific Assessment Report Series;* National, Ed.; National Water Research Institute Environment Canada: Burlington, ON, Canada, 2001; Vol. 1.

25. Susini, J.; Salome, M.; Fayard, B.; Ortega, R.; Kaulich, B. *Surf. Rev. Lett.* **2002,** 203-211.

# Chapter 5: General Conclusions

The work discussed here showcases three fields in which ICP-MS may be applied to analyze samples. Many of these applications highlight the continued growth of ICP-MS in an expanding number of fields.

Public safety is a main concern throughout the world today. Recent studies have indicated that there are surprising amounts of toxic elements, such as As, in food because they have largely gone unchecked and unregulated. Measurements of these toxins must be performed in order to determine global limits to keep the world food supply safe for human consumption.

A technique was developed and reported as a new tool for forensic scientists. There is limited sample destruction when a laser is utilized, which can preserve a large portion of the sample for additional analyses on the same piece of evidence. Combining additional statistical methods with the sensitivity of LA-ICP-MS can rapidly identify trace components in evidence that may otherwise be overlooked. Additionally, statistical techniques and LA-ICP-MS may be employed to rapidly determine if a piece of evidence from a crime scene can be distinguished from similar evidence collected elsewhere.

ICP-MS was also applied to the field of archaeology to identify pigments found at the site of a 325+ year-old shipwreck. Elemental analysis of these samples revealed clues to the common practice of trade that in the late 1600s, which was often dishonest and the products were unsafe. Many of the pigments intended for trade were adulterated with Pb to cheapen them, as learned 325 years later using modern science. Additionally, modern knowledge of

vermilion (HgS) reveals that the product itself was not safe for human exposure and certainly adulterating it with Pb made it even more harmful.

ICP-MS is one of the most sensitive useful tools for elemental analysis. A deeper understanding of the exact composition of various samples using ICP-MS can help scientists assist in setting new public safety standards in the present, provide new techniques for the future, and learn life in the past. The work highlighted here demonstrates that ICP-MS is a versatile technique that has led to even broader acceptance in an increasing number of fields.

## Acknowledgements

The work in chapter 3 was funded under a grant by the National Institute of Justice (award number: 2009-DN-R-112). Other research performed during my time in grad school was made possible by a grant from the U.S. Department of Energy, Office of Nuclear Nonproliferation (NA-22). Additional research was funded under and a Graduate Assistance in Areas of National Need (GAANN) fellowship from the department of chemistry at Iowa State University and the U.S. Department of Education.

I would like to thank Dr. R.S. Houk for his guidance and leadership throughout my graduate studies. I would also like to thank Stan Bajic and Dan Zamzow for their valuable conversations and daily help. I would like to thank reddit, for making it possible to bring together an archaeologist (Eric Ray), a geologist (Cameron Sheya), and a chemist to collaborate on the work described in chapter 4. I would like to thank Nathan Saetveit for providing me with the introductory knowledge of project material and ICP-MS. I would also like to thank Travis Witte and Chris Ebert for their breadth and depth of knowledge, assistance over the years with anything I needed, and their close friendship that was essential to keeping me going on a daily basis. Furthermore, I would like to thank all present and past Houk Group members for valuable conversations throughout the years.

I would like to thank my mom Jan Mekoli and my brother Mitch Mekoli for supporting me my whole life. They are my two amigos and I am so very lucky to have them in my life. Finally, I would like to thank my husband, Alex Shaver, who is an unwavering source of love and support and I am lucky to have him by my side. His constant encouragement and optimism are what helped me get through the difficult years of my graduate studies.